MAGNETIC PROPERTIES OF $Fe_{1-x}Co_xAs$

BY

FARES SUBAIT HADI OBAD

A Thesis Presented to the

DEANSHIP OF GRADUATE STUDIES

KING FAHD UNIVERSITY OF PETROLEUM & MINERALS

DHAHRAN, SAUDI ARABIA

In Partial Fulfillment of the

Requirements for the Degree of

MASTER OF SCIENCE

In

PHYSICS

DECEMBER, 2017

KING FAHD UNIVERSITY OF PETROLEUM & MINERALS

DHAHRAN- 31261, SAUDI ARABIA

DEANSHIP OF GRADUATE STUDIES

This thesis, written by **Fares Subait Hadi Obad** under the direction his thesis advisor and approved by his thesis committee, has been presented and accepted by the Dean of Graduate Studies, in partial fulfillment of the requirements for the degree of **MASTER OF SCIENCE IN PHYSICS.**

Dr. Khalil A. Ziq
(Advisor)

Dr. Abdullah A. Al-Sunaidi
Department Chairman

Dr. Muhammad Baseer Haider
(Member)

Dr. Salam A. Zummo
Dean of Graduate Studies

Dr. Saleem Rao
(Member)

28/12/17

Date

I would like to dedicate this thesis to my loving parents

To my brothers and sisters

To my wife and my children

ACKNOWLEDGMENTS

Firstly, I would like to express my sincere gratitude to my supervisor, Professor Dr. Khalil A. Ziq for the availability while developing the project. For his patience, motivation, and vast knowledge. I also appreciate the patience exhibited by all the member of the committee during the course of undergoing this thesis work.

I would like to thank KFUPM institution for the scholarship granted to me to embark on my MSc. degree program. I would also like to extend my gratefulness to the erudite faculty members of Physics Department for the paradoxical rigorous and appealing training in the discipline to complement my physics background.

Finally, I would like to thank all my family and friends who helped me to be what I am today.

TABLE OF CONTENTS

LIST OF TABLES

LIST OF FIGURES

LIST OF ABBREVIATIONS

LIA	:	Lock-In Amplifier
FWHM	:	Fill Width at Half Maximum
FC	:	The Field-Cooled
ZFC	:	The Zero-Field-Cooled

ABSTRACT

Full Name : Fares Subait Hadi Obad

Thesis Title : Magnetic Properties of Fe(1-x)Co(x)As

Major Field : Physics Department

Date of Degree : December, 2017

In this thesis, we present a new improved ac-susceptometer that was used to investigate the magnetic state of $Fe_{1-x}Co_xAs$. In particular, we measured the total susceptibility χ and the often-ignored lag-angle $\Delta\varphi$ between the magnetization and the applied ac-field. All measurements reveal an antiferromagnetic maximum at the Neel's temperature T_N that shifts to higher values with increasing cobalt-substation. Moreover, the full width at half-maximum (FWHM) increases as cobalt-substation increase which indicates that the helimagnetic modes in pure FeAs extend slightly into to the normal antiferromagnetic behaviour. The lag-angle $\Delta\varphi$ revealed at temperature T_P that shifts to higher values with increasing frequency. This phenomenon was used to investigate the activation energy (U_0). We found out that the activation energy obeys the Arrhenius plot of ($ln\ f$ vs. $1/T_P$) at low frequency. At high frequency, the activation energy deviate from an Arrhenius law to the Vogel–Fulcher law.

ملخص الرسالة

الاسم الكامل: فارس سبيت هادي عباد

عنوان الرسالة: الخواص المغناطيسية ل $Fe_{1-x}Co_xAs$

التخصص: فيزياء

تاريخ الدرجة العلمية:December, 2017

في هذه الرسالة، استخدمنا نظام جديد ومطور من الملفات لدراسة الخواص المغناطيسية لزرنيخ الحديد (FeAs) المطعم بالكوبالت. قمنا بقياس القابلية المغناطيسية والفرق في زاوية الطور بين المغنطة (Magnetization) والمجال المغناطيسي المتردد والمطبق على العينات. اظهرت القياسات أن حالة المادة المغناطيسية تتحول من البارامغناطيسية الى الانتيفيرومغناطيسية عند درجة حرارة معينه تسمى (Neel's temperature T_N) والتي بدورها تزداد بزيادة تركيز الكوبالت. بالإضافة الى ذلك وجدنا ان اتساع القمة الحرارية يزداد بزيادة تركيز الكوبالت وهذ يدل على ان التركيب الحلزوني المغناطيسي للمادة بدأ ينهار. عند دراسة زاوية الطور واعتمادها على التردد، بينت النتائج وجود قمة عند درجة حرارة (Tp) واتى يبدأ بالا نزياح الى الأعلى مع زيادة الترد حيث تم استخدام هذه الظاهرة لحساب الطاقة اللازمة للتفعيل أثناء التغير في طور المادة.

CHAPTER 1

INTRODUCTION

Materials present many physical properties that were used in a wide range of applications. These properties are studied to properly characterize these materials and explore their possible use for specific practical application. Among these properties, the ones studied in this work are the magnetic properties of $Fe_{1-x}Co_xAs$ [1,2].

Interests in these old-new materials are mainly exited by the recent discovery of superconductivity in iron-based compounds [3]. Primary systems are Iron mono-arsenide (FeAs) including oxypnictides.

The orthorhombic MnP-type structure (Figure1) of FeAs was first studied by Hägg, resolved by Fylking [4] and with details investigation by Selte et al. The determined lattice parameters are: $a = 5.440$ Å, $b = 6.026$ Å, $c = 3.371$ Å. Upon cooling, a paramagnetic to antiferromagnetic transition was observed near Neel temperature T_N 77K [5,6]. Further investigation by Morifuji and Motizuki revealed that the orthorhombic MnP-type structure of FeAs attains a double helical magnet ordering along the c-axis below T_N [7]. More recently Ando et al. used iodine vapor transport method to prepare single crystals and investigated their magnetic and transport properties. Their measurements revealed a kink in the susceptibility and in the resistivity near 70K[8].

Specifically, the susceptibility showed a kink at 70K in the *a* and *b*-directions but not in the *c*-direction [9].

Ziq et al, also studied FeAs single crystals vapor grown by two different methods and found that the magnetic phase is greatly affected by the purity of crystals [12]. Rodriguez al., had reported T_N of 69.6(1)K in agreement with the value obtained by Ando [10]. Similar result was found using the heat capacity [8,10].

The crystal structure of CoAs was first studied by Fylking and with details determined by Selte et al. They found that CoAs adopts the orthorhombic MnP-type structure and the unit cell dimensions are: a=5.2867(11) Å, b=5.8682(14) Å, c=3.4892(8) Å [36].

The similarity between the crystal structure of CoAs and FeAs and the atomic size of Fe and Co makes cobalt suitable candidate for doping into FeAs. The same structure was found for $Fe_{1-x}Co_xAs$ at and below room temperature, but at $x = 0.03$ the helical magnetic structure is becoming easier to destroy with increasing Co-substitution [12].
The Thesis is divided into 6-chapters:

1- Introduction
2- Experimental Techniques

   Results are discussed in 3, 4 and 5 chapters.
3- The Total Susceptibility
4- The Lag-angle Between the Magnetization and the *ac*-Field.
5- Activation Energy
6- Conclusion

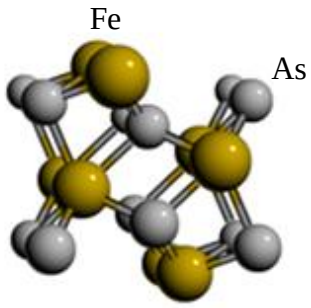

MnP-type Structure

Figure 1 The orthorhombic crystal structure of MnP-type

[https://homepage.univie.ac.at/michael.leitner/lattice/struk/b31.html]

1.1 Magnetism and Magnetic Properties

Magnetism is a quantum mechanical phenomena that is largely due to the atomic spins and their various exchange interactions. The “classical” orbital motion of the electrons creates an orbital magnetic moment that aligns with the magnetic field. The spins of the electrons provide the main contribution to the atomic magnetic moment in accordance with Hund’s rules. Therefore, the net of atomic magnetic moment consists of both orbital and spin magnetic moment see (Figure 2) [13,14].

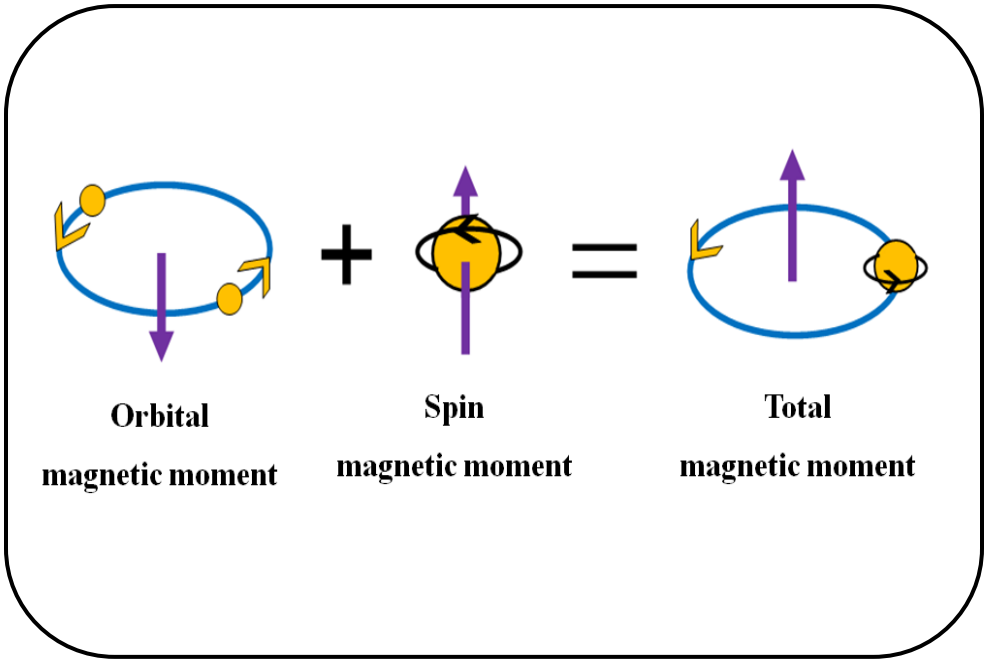

Figure 2 The Origin of Magnetism

1.1.1 Magnetic Field Vector

The magnetic field (*H*) that is commonly used to investigate the magnetic properties of various materials is commonly generated by current (*I*) in a coil. The relation between the field and the current is:

$$H = \frac{N}{l} I \tag{1.1}$$

where *N* is number of turns over length *l*.

Since the magnetic field is always induced in different environments, the way the magnetic field strength interacts with it comes as:

$$B = \mu H \tag{1.2}$$

Where μ is the permeability of the environment and is related to the vacuum permeability by a ratio of the material permeability called relative permeability:

$$\mu = \mu_r \mu_0 \tag{1.3}$$

Where μ_{r} is the relative permeability and $\mu_0 = 4\pi \times 10^{-7}\,\mathrm{H/m}$, corresponding to the vacuum permeability [14].

1.1.2 Magnetization

The magnetization *M* of a material is the net of magnetic dipole moment per unit volume:

$$M = \frac{1}{V} \sum_i \mu_i \tag{1.4}$$

The magnetization of the sample (M) adds up to the applied magnetic field (H_{ap}) giving rise to the magnetic induction (B) or the total magnetization. The demagnetization field (H_d) tends to reduce the net internal magnetic field (Hi), it is given as:

$Hi=H_{ap}+ H_d$, where $H_d=NM$ and N is the demagnetization factor that depends on the geometry of the sample. For small field, H_d is often neglected and $Hi=H_{ap}=H$, we have:

$$B = \mu_o (H + M) \tag{1.5}$$

1.1.3 Magnetic susceptibility

The magnetic susceptibility represents the response of the magnetization to the external field; namely:

$$\chi = dM/dH \tag{1.6}$$

where χ is a dimensionless variable that represents the magnetic susceptibility of the material and can take positive or negative values depending on the substance [14]. The susceptibility can be approximated as $\chi = M/H$, then we have:

$$B = \mu_o (1 + \chi) H \tag{1.7}$$

The permeability of the material is:

$$\mu = \mu_o (1 + \chi) \tag{1.8}$$

and the relative permeability is

$$\mu_r = \frac{\mu}{\mu_0} = (1 + \chi) \tag{1.9}$$

1.2 Types of magnetic materials

The response of the susceptibility to temperature variation can be used to classify magnetic materials to various magnetic phases [14,15]**.**

1.2.1 Diamagnetism and Paramagnetism

Diamagnetic material is characterized by "small < -10^{-5} in SI-units" negative susceptibility. According to Eq.(1.7), the magnetization opposes the applied magnetic field. However, the susceptibility of paramagnetic materials is also small but positive (~10^{-5}). The magnetization is along the direction of the applied magnetic field [14-16]. Both susceptibilities decrease with increasing temperature.

1.2.2 Ferromagnetism

This is the strongest type of magnetism found in materials due to its permanent magnetization in the absence of a magnetic field. The origin of this strong magnetism is the presence of a spontaneous magnetization produced by a parallel alignment of spins and the state of magnetic domains (Figure4). As the temperature increases, the spontaneous magnetization vanishes at certain temperature which is called the Curie point (θ). The susceptibility is inversely proportional with $(T-\theta)$. This is called *Curie-Weiss law.*

$$\chi = \frac{C}{T-\theta} \qquad (1.10)$$

Iron and cobalt are examples of ferromagnetic transition above room temperature [15], Gadolinium is rare earth ferromagnetic element with transition near room temperature.

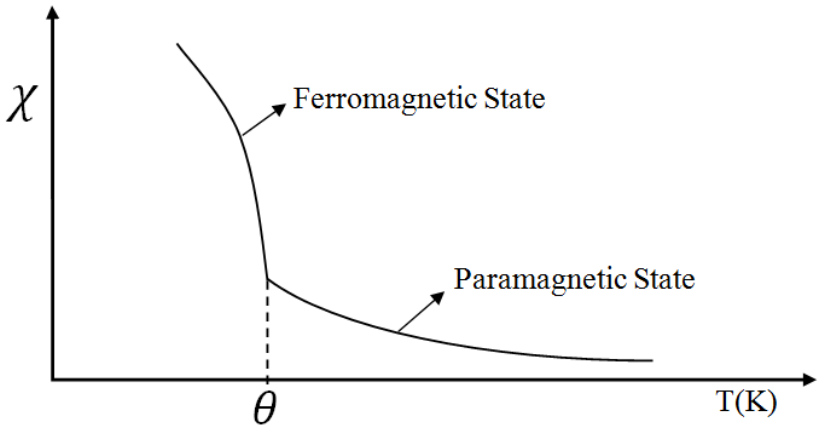

Figure 3 Temperature dependence of the susceptibility of ferromagnetic materials

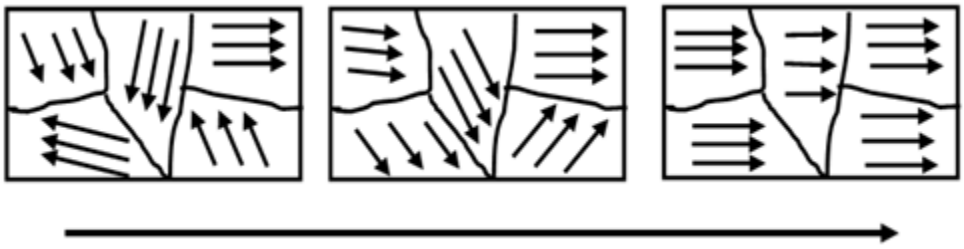

Figure 4 Behavior of a ferromagnetic material to an applied magnetic field. The arrow indicates the direction of increasing magnetic field or decreasing temperature.

1.2.3 Antiferromagnetism

Antiferromagnetic materials show very low magnetism at intermediate magnetic (~ k Oe) as they have no spontaneous magnetic moment, their atomic spins are antiparallel. Antiferromagnetic materials have a small positive susceptibility at all temperatures. When an external magnetic field is applied, the susceptibility increases as the temperature increases reaching a maximum value at a characteristic transition temperature known as the Neel temperature (T_N), contrary to the case of the normal paramagnet. Above T_N the susceptibility decreases and the spin ordering disappears completely (Figure 5). Below T_N, the material is antiferromagnetic and transforms to paramagnetic above T_N [13,15].

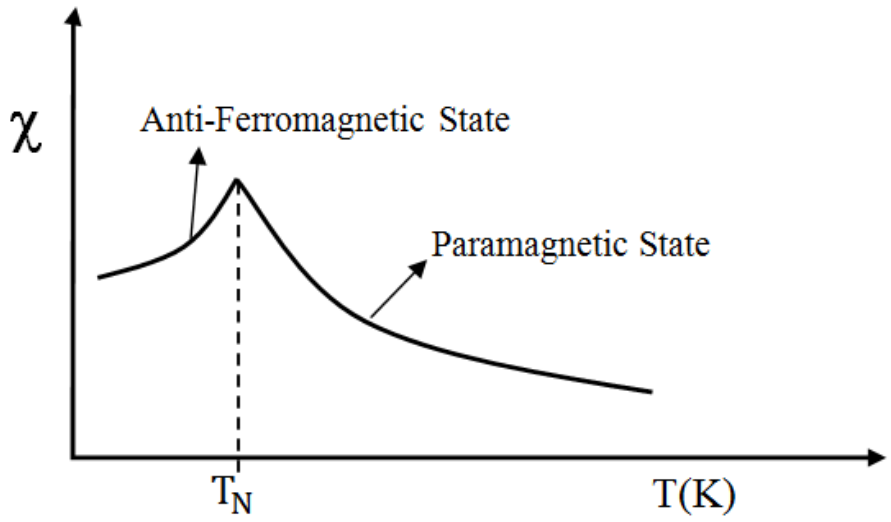

Figure 5 Temperature dependence of the susceptibility of antiferromagnetic materials

1.3 AC Magnetic Measurement

The magnetic susceptibility can be measured by two complementary methods the *dc* and *ac* techniques.

DC measurements (*dc* techniques) determine the equilibrium magnetization of a sample when a small static magnetic field (10's Oe- few kOe) is applied, and the magnetization is measured as the temperature varies. The *dc*, or static, susceptibility is then given by:

$$\chi_{dc} = \frac{M}{H_{dc}} \qquad (1.11)$$

The measured units of *M* and *H* are the same which is amperes per meter, so the susceptibility is dimensionless.

Unlike DC magnetometry, in AC measurements (*ac* techniques) the applied field is driven by a small *ac*-current, causing a time-dependent moment in the sample. This time dependence is able to induce an electric current in the pickup coil, allowing measurements of the magnetization of a static sample [16]. This method also offers the opportunity to investigate the dependence of ac-susceptibility on frequency. The sensitivity of the *ac*-susceptibility typically surpasses that of *dc*-techniques [17]

In the limit of low frequencies, where a comparison with dc measurements is possible and the applied ac field $H_{ac} = H_{ao} cos\omega t$, the time-dependent moment can be expressed by:

$$M_{ac} = \frac{dM}{dH} H_{ac} cos(\omega t) \qquad (1.12)$$

where H_{ac} is the amplitude of the applied field, ω is the driving frequency, and the susceptibility χ of the sample is represented by (dM/dH_{ac}) which is the slope of the M(H) curve.

In the limit of high frequency, the magnetic moment of the sample is not able to follow the driving field and starts to lag behind. This effect is sensed by the detection circuitry ending in the measurement of two quantities: the magnitude of susceptibility (χ) and the phase shift due to the sample lag, φ relative to the driving signal.

AC susceptibility has an in-phase component (χ') also known as real component, and an out-of-phase component (χ'') or imaginary component:

$$\chi = \chi' + i\chi'' \tag{1.13}$$

The magnitude and the phase shift are related to χ' and χ'' by the following relations:

$$\begin{aligned} \chi' &= \chi \cos\varphi \\ \chi'' &= \chi \sin\varphi \end{aligned} \quad \Longleftrightarrow \quad \begin{aligned} \chi &= \sqrt{\chi'^2 + \chi''^2} \\ \varphi &= \arctan\left(\frac{\chi''}{\chi'}\right) \end{aligned} \tag{1.14}$$

The imaginary component χ'' indicates dissipative processes occurring in the sample, that have different causes for each material measured. Different measurement processes access different information and the most used measurements are [16,18]:

- χ vs. Temperature
- χ vs. Driving frequency
- χ vs. DC field bias
- χ vs. AC field amplitude
- Harmonic measurements

1.3.1 AC susceptometer

The susceptometer for ac measurements usually has a configuration with two primary coils coaxially wound over the two secondary, pickup, coils wound in opposite directions and electrically connected in series see (Figure 6). The primary coil, or excitation coil, should produce a near-uniform ac magnetic field. As the pickup coils are wound in opposition, the total magnetic flux induced, without sample and from unwanted external sources, is ideally zero since one of the coils generates a current with the same magnitude and opposite direction of the other one, meaning an equilibrium state is achieved.

When the sample is placed at the center of one of the pickup coils the equilibrium state will be broken and the measured rms voltage sensed across the secondary coils will be:

$$v(t) = -\frac{d\Phi}{dt} \qquad (1.15)$$

which is related to the sample response and is dependent on time due to the ac field. This induced voltage proportional to the magnetization of the sample which is given by:

$$v(t) = -Ll\frac{dM}{dt} \qquad (1.16)$$

Where L is the mutual inductance per solenoid primary turn and l is the length of the primary coil. According to $M = \chi H$ and the applied ac field $H_{ac} = H_{ao}cos\omega t$ we get: $v_{rms} = 2\pi LlfH_{rms}\chi$, this is the measured voltage at the empty coil. When a sample is placed within one of the pickup coils the voltage balance is disturbed and proportional to the amplitude of the ac susceptibility of the sample and other parameters. Thus

$$v = \left(\frac{1}{\alpha}\right)VfH_a\chi \qquad (1.17)$$

Where v is the voltage, α is the calibration constant, V is the volume of sample and f and H_a are the frequency and magnitude of the applied magnetic field [19].

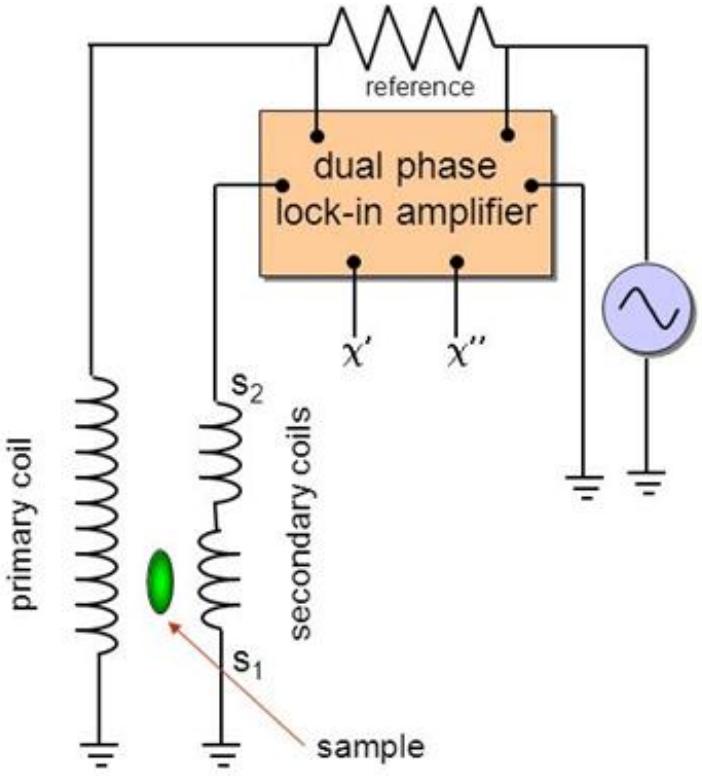

Figure 6 Coil configuration of the AC Susceptometer

1.4 Literature review

1.4.1 Magnetic properties of FeAs

Recently a series of iron-based compounds is found to be a new kind of high-temperature superconductors [3]. The fundamental building block in these systems is FeAs layers in a way similar to the CuO layer in high temperature superconductors. On its own, FeAs is non-superconducting down to very low temperatures (~1K). Moreover, applying high pressure (25 GPa) did not induce superconductivity nor any structural transformation in this compound [20]**.** This is unlike another similar material CrAs, where superconductivity is induced near 2K under external pressure. At room temperature, FeAs is paramagnetic and undergoes a transition into an anti-ferromagnetic (AFM) state near 70K.

The structure of FeAs was first studied by Hägg who found that it was orthorhombic and related to that of NiAs. Later, FeAs was shown to be isostructural with orthorhombic MnP-type (Figure1) and the double helimagnetic ordering along the c-axis [11]. Selte et al, also investigated the magnetic structure of FeAs in the early 1970s using neutron diffraction, magnetic susceptibility, X-ray and differential thermal analysis.

The crystal structure is found to be essentially of the MnP-type and shows an interesting helimagnetic structure which disappears at ~ 77K. The primitive unit cell contains eight atoms, 4Fe and 4As in the position of $x = 0.0027 \pm 0.0005$, $y = 0.1994 \pm 0.0005$, $z = 1/4$ for Fe and $x = 0.1992(4)$, $y = 0.5773(4)$, $z = 0.264(3)$ for As.

The unit cell dimensions are: $a = 5.4420(7)$ Å, $b = 6.0278(7)$ Å, $c = 3.3727(6)$ Å. The unit cell dimensions and positional parameters for FeAs are approximately independent of temperature up to ~ 1300k. The magnetic susceptibility of (FeAs) [4.2-1000 K in field up to 15 kOe] along the b-axis was substantially lower than the a-axis susceptibility and satisfies the Curie-Weiss Law between ~ 300-650K. Powder neutron diffraction measurements [12-293 K] revealed that FeAs undergoes a long-range antiferromagnetic ordered state at $T_N = 77 \pm 1$ K [5,6].

Ando et al., using Iodine vapor transport method to prepare the single crystal of FeAs. The susceptibility and the resistivity showed a kink near 70 K. At low temperature, the difference between the field-cooled (FC) and zero-field-cooled (ZFC) data is observed only in χ_C, which indicates that some antiferromagnetic domains are formed in the helimagnetic ordered phase. The obtained lattice constants are $a = 5.440$ Å, $b = 6.026$ Å, $c = 3.371$ Å, in agreement with polycrystalline sample results obtained earlier. They confirmed that with higher purity of Fe and As, T_N does not change [8].

Rodriguez et al., had reported T_N, using Powder neutron diffraction, of 69.6 K which is much closer to the value obtained by the magnetic susceptibility measurements of Segawa and Ando and show that the helical picture best describes the magnetic ordering

from 15 K up to T_N. It was found that the moment along the b-axis is about 15 % larger than along the a-axis [10]. A. Błachowski et al. investigated FeAs by transmission Fe Mössbauer spectroscopy in the temperature range 4.2 – 1000 K. The primarily transition to the paramagnetic state was in the a-c plane at 69.2 K [21]. The heat capacity of FeAs has been determined by adiabatic calorimetry from 5 to 1030 K. The transition is observed at T_N= (70.95 $\pm$0.02)K marking the disappearance of the double helical magnet ordering along the c-axis above T_N [11]. These discrepancies in T_N are within the experimental error [8].

1.4.2 The effect of doping cobalt (Co)

Superconductivity seems to appear when the antiferromagnetic phase is suppressed in certain parent compound. This motivated the search for superconductivity in FeAs when doped with elements that may suppress or destroy the antiferromagnetic helical ordering [8]. Cobalt atoms directly replace iron atoms in a random distribution across the lattice. This means macroscopic properties of $Fe_{1-x}Co_xAs$ should vary smoothly between end members (FeAs and CoAs). Cobalt doping is found to induce superconductivity in $BaFe_2As_2$, with the optimum doping close to 6% cobalt- at the Fe site [22].

The magnetic properties of CoAs were first studied by Fylking and with details determined by Selte et al. The CoAs phase has been investigated by the neutron diffraction, magnetic susceptibility, X-ray and diffuse reflectance measurements. At room temperature, the structure of CoAs adopts the orthorhombic MnP-type. The unit cell contains 4Co and 4As with x=0.0023(10), y=0.2000(5), z=1/4 for Co, x=0.1996(7), y=0.5869(3), z=0.2716(22) for As, and the unit cell dimensions are: a=5.2867(11) Å, b=5.8682(14) Å, c=3.4892(8) Å. The structure of CoAs remains unchanged between

liquid helium temperature and room temperature. The magnetic susceptibility dependence of the temperature of CoAs exhibit a Curie-Weiss Law above 490k with $\theta = -230 \pm 40$K [36].

Selte et al. investigated in details several properties of pure FeAs and cobalt doped $Fe_{1-x}Co_xAs$ for $0 \leq x \leq 1$ [12]. Neutron diffraction and X-ray data confirm the MnP-type structure of $Fe_{1-x}Co_xAs$ for $0 \leq x \leq 1$, but the double c-axis helimagnetic ordering in pure FeAs extends slightly into the ternary regions close to $x = 0.03$. They measured the magnetic susceptibility and observed several different regimes at higher temperatures (above 300 K), which may be due to the magnetic moments at the cobalt and iron atoms. No significant secondary phase has been detected. Apart from FeAs (~ 300-650K), the $Fe_{1-x}Co_xAs$ samples do not satisfy the Curie-Weiss Law [12].

1.4.3 The dependence of ac-susceptibility on frequency

AC-measurement is a widely used technique to study the Magnetic (χ vs T) and Transport (ρ vs. T) properties of materials. Real ($\chi'(T)$ and imaginary $\chi''(T)$ components are associated with ac-measuring techniques. Both components of ac-susceptibility may depend on the applied frequency. The dependence of ac-susceptibility on frequency is commonly used to probe the magnetic relaxation by determining the relaxation time (τ) and the activation energy using the following models:

- The Vogel-Fulcher law:

$$\tau(T) = \tau_0 \exp\left(\frac{\Delta E}{k_B(T-T_0)}\right) \qquad (1.18)$$

- The generalized Vogel-Fulcher law:

$$\tau(T) = \tau_0 \exp\left(\frac{\Delta E}{k_B (T - T_0)^z}\right) \quad (1.19)$$

- The Arrhenius law :

$$\tau(T) = \tau_0 \exp\left(\frac{\Delta E}{k_B T}\right) \iff lnf = \frac{-\Delta E}{k_B}\frac{1}{\mathrm{T}} + \ln f_0 \quad (1.20)$$

ΔE is the activation energy (energy barrier) given as $\Delta E = E_a =$ KV which is related to the anisotropy constant K, V is the volume of the relaxing particle and $k_B T$ is the thermal energy. The slope of Arrhenius plot of (lnf vs. 1/T) equal $\frac{-\Delta E}{k_B}$ and f_0 is a characteristic frequency of the material.

The measurement of $\chi'(T)$ and $\chi''(T)$ often reveals a peak with temperature (T_P) that may shift to lower or upper temperature as the frequency decreases. The Arrhenius plot of lnf vs. $1/T_P$ gives the value of the activation energy ΔE [16,23-26]. For example, for a family of molecular chains magnets based on Mn-porphyrin and TCNE-radical [MnTPP][TCNE] (TPP=tetraphenylporphyrin,TCNE=tetracyanoethylene) show mixed ferromagnetic and spin-glass-like behavior. In the single chain magnet [MnF_4TPP][TCNE], T_P shifts to higher temperature as the frequency increase and $\Delta E = 117 k_B T$ [27-29]. Similar results were found in $Cu_{1-x}Mn_x$ spin-glass, ceramic $Bi_{1.6}Pb_{0.4}$ -$Sr_2(Ca_{1-x}Nd_x)_2Cu_3O_\delta$ and (γ-Fe_2O_3) nanoparticles nano particles material [30,31].

In this thesis, we will use our improved design of an ac-susceptometer to investigate the magnetic properties of $Fe_{1-x}Co_xAs$ at low temperatures as results of cobalt-substation. In particular, we are interested in low concentration of Co (≤ 0.05) where no magnetic ordering was observed. Moreover; Co-doping destroys the helical structure observed in FeAs as has been revealed by neutron diffraction measurements for x=0.05 compound, Selte et al. theorized that the transition would be suppressed at a doping fraction close to 0.03 [13].

CHAPTER 2

EXPERIMENTAL TECHNIQUE

2.1 Sample Preparation

Single and polycrystalline of $Fe_{1-x}Co_xAs$ have been prepared using solid state reaction, iodine vapor transport, and Bridgman methods. High purity (~99.99%) Fe, Co and As elements are mixed in atomic ratio to prepare the polycrystalline materials. The powder was mixed, grinded and sealed under partial Argon pressure in quartz tube. Tubes were annealed at various temperature protocols to obtain good quality samples [8,32].

(1) Iodine Transport Method:

- About 100 mg of $Fe_{1-x}Co_xAs$ powder are sealed in a 20-30 cm long quartz tubes along with few milligrams of Iodine. The volume of the tube is used to determines the amount of iodine. At the growth temperature, the internal pressure inside the tube (due to iodine vapor) is kept below the atmospheric pressure.
- The sample side of the quartz tube is kept at about 800 °C and the growth end is at about 600-700°C for two weeks.
- This method often yields crystals with few mm in size.

(2) Bridgman flux method:

- About 2 grams of $Fe_{1-x}Co_xAs$ polycrystalline powder was sealed in double quartz tubes under partial Argon pressure.
- Samples were melted at 1100 °C, kept for several hours, and then slowly cooled at a rate of about 5°C/h to about 500°C.

2.2 Experimental setup

As a whole, the system we implemented for *ac*-susceptometer has a rather simple setup with a few key components that provide a good experimental environment. The system is briefly described in the following (Figure 7):

- **Cryostat**

A cryostat used hots several experimental setups; *ac*-susceptibility, *ac and dc*-resistivity setups. The measuring temperature range is 4-325K. The system consists of four different main parts: turbo-molecular Pump, temperature controller, Compressor, and closed cycle refrigerator.

- **Lock-in Amplifier(*LIA*)**

This equipment is very useful in AC susceptibility measurements due to its ability to isolate real and imaginary components the susceptibility. In this setup, we used DSP Lock-In Amplifier (*LIA*) model SR830 from Stanford Research Systems. This device meets two requirements of this system: provides a current source to feed the primary susceptometer coil as well as an input module able to sense the potential difference from the secondary coil and deliver it to the computer, after suitable filtering and amplification.

- **Temperature Controller**

For the control of the cryostat temperature, we use a LakeShore Model 336 Temperature Controller.

- **Computer**

The computer is used for the data acquisition and storage.

2.3 Design of AC Susceptometer

For these experiments, the susceptometer coil consists of two primary coils on the outside and two secondary coils inside. It was wounded in two non-magnetic low temperature plastic tubes with a length of 1 cm and a 3 mm (Figure 8). The secondary coil was wounded first over the tube with 12 layers and the primary was wound over that with 10 layers in each coil (Figure 8,9). The total number of turns are: secondary coil has 535 turns in each coil; the primary with 370 turns in each coil. The field in the coil can be easily calculated. For an infinite solenoid, the field (in gauss) is given by $B = \mu_O nI$, but for a finite coil, this is modified to include a pre-factor based upon the coil's dimensions [33-35].

$$B = \left(\frac{L}{\sqrt{d^2+L^2}}\right)\mu_O nI \qquad (2.1)$$

where $n = N/L$ is the number of turns per unit length (N is the number of turns in the primary coil, and L is the total length of the coil. I is the current and d is the average diameter of the primary coil.

By using the data in table 2 to determine the field which induced by the primary coil:

$$\frac{B}{I} \approx 0.05\ \frac{T}{A} = 0.5\ Oe/mA \qquad (2.2)$$

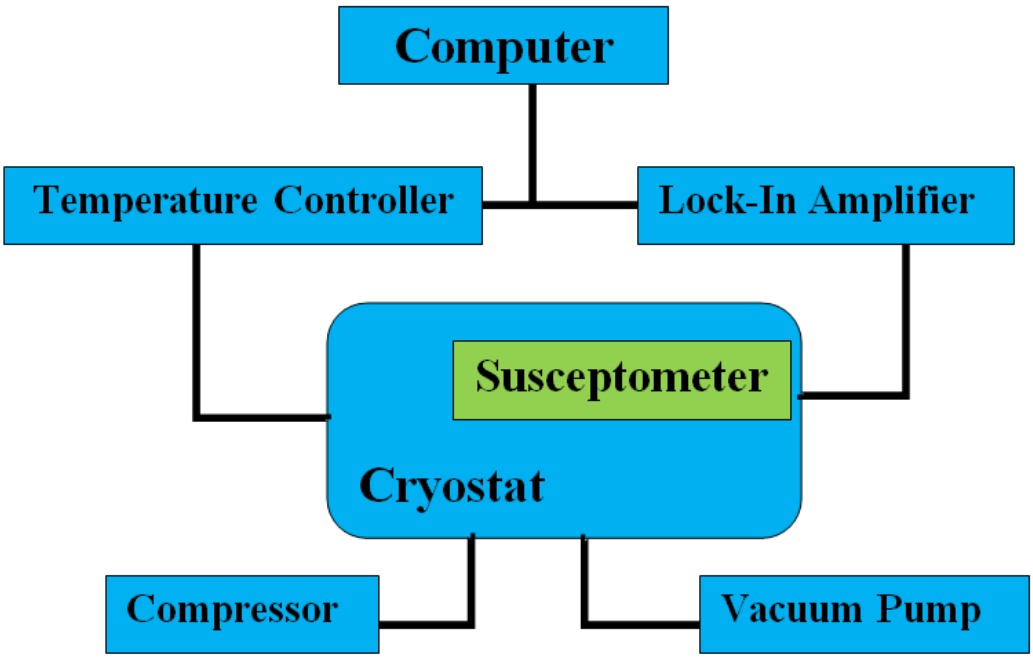

Figure 7 System Set-up for the AC susceptibility measurements

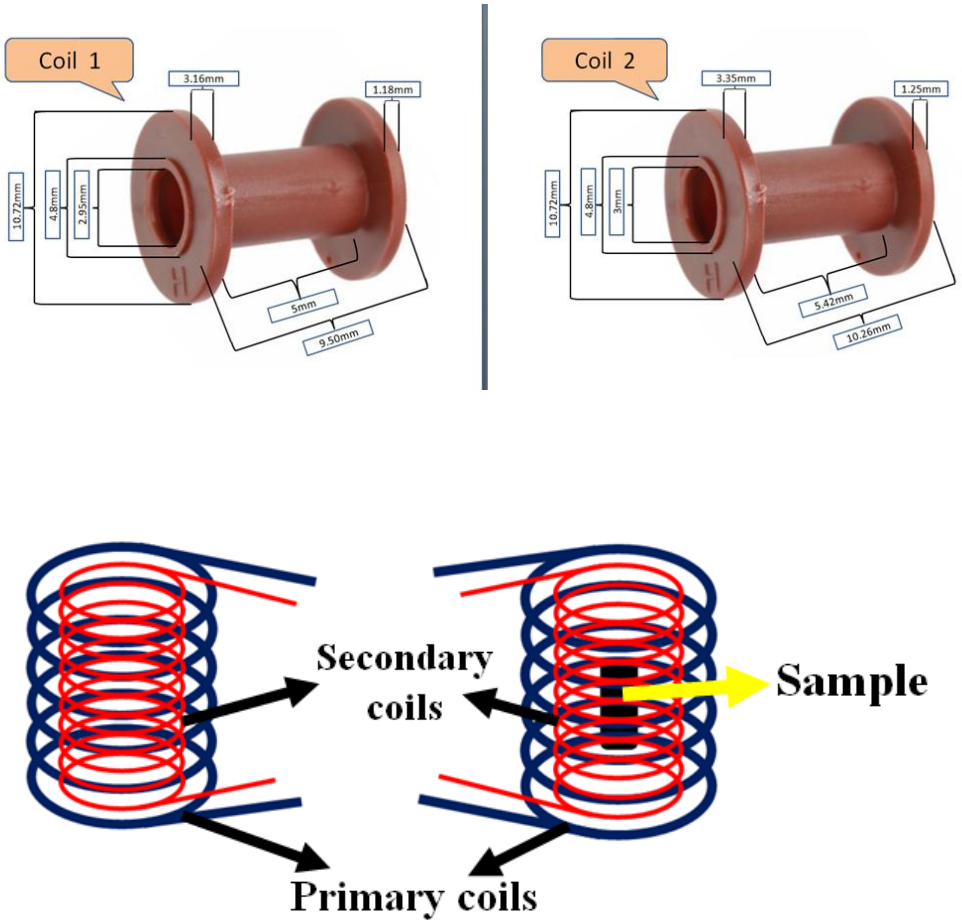

Figure 8 The coils dimensions

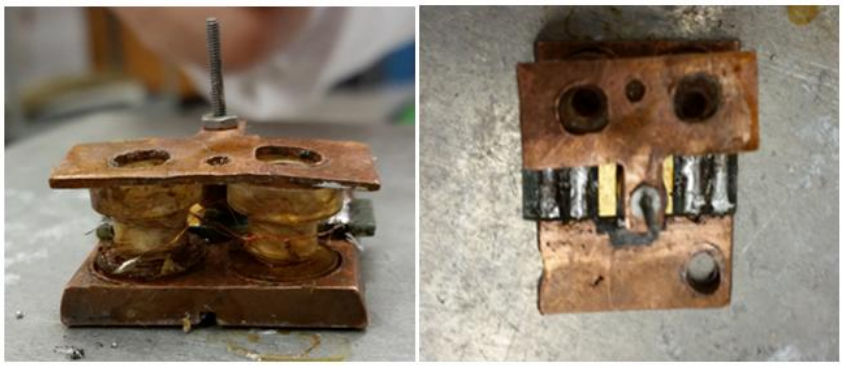

Figure 9 Real coils

Table 1 Parameters of coils

	Secondary Coil		**Primary Coil**	
	Coil 1	**Coil 2**	**Coil 1**	**Coil 2**
Wire Diameter	100 μm	100 μm	63 μm	63 μm
Number of turns	92 turns	92 turns	148 turns	150 turns
Resistivity	5.3 Ω	5.3 Ω	19.6 Ω	23.9 Ω
Number of layers	2 layers	2 layers	2 layers	3 layers

Table 2 Parameters of updated coils

	Secondary Coil		**Primary Coil**	
	Coil 1	**Coil 2**	**Coil 1**	**Coil 2**
Wire Diameter	0.1007 mm	0.1007 mm	0.1270 mm	0.1270 mm
Number of turns	535 turns	535 turns	~370 turns	~370 turns
Resistivity	23.3 Ω	23.8 Ω	12 Ω	11.4 Ω
Number of layers	12 layers	12 layers	10 layers	10 layers

CHAPTER 3

THE TOTAL SUSCEPTIBILITY

AC total susceptibility is a complex value and given by:

$$\chi = \chi' + i\chi'' \tag{3.1}$$

The magnitude of the total susceptibility is related to χ' and χ'' by the following relations:

$$\chi' = \chi\, cos\varphi, \qquad \chi'' = \chi\, sin\varphi \longrightarrow \chi = \sqrt{\chi'^2 + \chi''^2} \tag{3.2}$$

Where χ' is the real component that stays in-phase with the oscillating field and related to the reversible magnetization process; while χ'' is the imaginary part that is out-of-phase with the oscillating applied magnetic field. The imaginary part is related to energy losses due to the irreversible variations of the magnetization with the applied field or temperature changes. Perhaps one of the most important advantages of the ac susceptibility measurement using the *LIA* is measure both components of the total susceptibility and the lag angle. To measure both components, we use the phase adjust feature on the *LIA* to separate the real and imaginary components of χ, φ. The χ' is proportional to the signal measured at φ, and the χ'' is proportional to the signal measured at $\varphi + 90$.

$$V' = v_0 cos\varphi + v_{90} sin\varphi \tag{3.3}$$

$$V'' = v_{90} cos\varphi - v_0 \, sin\varphi \qquad (3.4)$$

Where V' is the in-phase voltage (φ), and V'' is the out-of-phase voltage ($\varphi + 90$). v_0 and v_{90} are the *LAC* voltage at 0° and 90° [19].

3.1 FeAs single crystal

Single crystals grown by the iodine vapor growth are very small in sizes (1X2X0.1mm^3). The ac-signal is very small (due to the small filling coil factor) comparable to the background signal. However, the dc-magnetic susceptibility can be measured in a relatively large dc-field. The dc-susceptibility is shown in figure (10) with field (0.1T) applied parallel to the *ab*-plane. The figure revels that the field cooled and the zero field cooled curve coincides on top of each other with an inflection point near 75K as marked by the arrow. Measurements at higher magnetic field (5T) is shown in figure (11). The figure shows that the transition inflection point is clearly shifted closer to 71K, in agreement with earlier published results. The hysteresis loop measured at 5K is shown in Fig. 12. The figure shows ferromagnetic behavior of the magnetization, confirming the ferromagnetic phase of FeAs crystal.

Moreover, we attempted to use the ac-susceptibility on these single crystals, the results were not satisfactory. An example of such measurements is shown in figure (13). The dependence of the lag-angle $\Delta\varphi$ (phase shift) on the temperature of single crystal shows very week signal and we were not able to get any stable measurements. Fluctuations dominated the measurements even after subtracting the background signal. But in general, the phase shift drops below ~ 38K and above ~ 150K. A minimum in the lag-angle occurs in the temperature range $38\text{K} \sim 150\text{K}$ at ~ 79.3K (Fig. 13) which is higher

than the value reported in the literature by Selte et al. The weak single crystals lead us to study larger polycrystalline of FeAs and $Fe_{1-x}Co_xAs$.

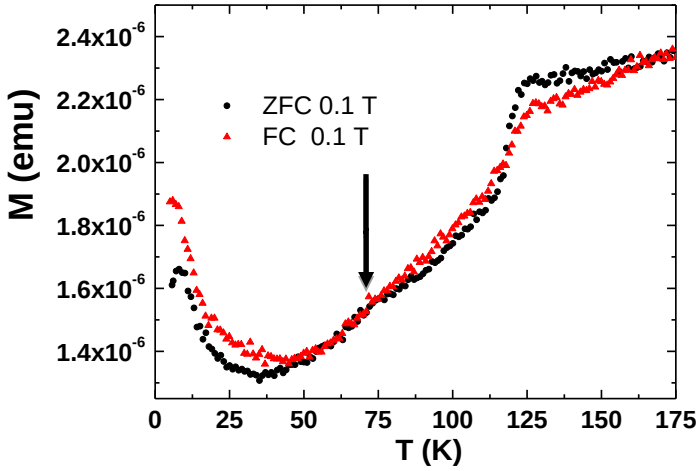

Figure 10 The dc-susceptibility for FeAs single crystal; Field cooled and zero field cooled (H=0.1T) susceptibilities are shown.

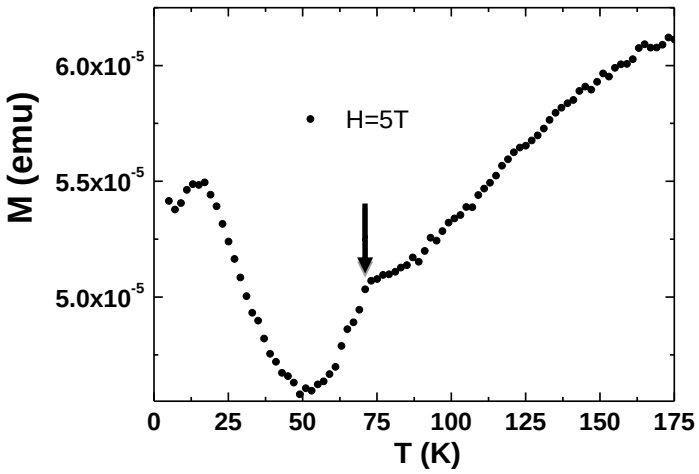

Figure 11 The dc-susceptibility measures in 5T field for FeAs single crystal.

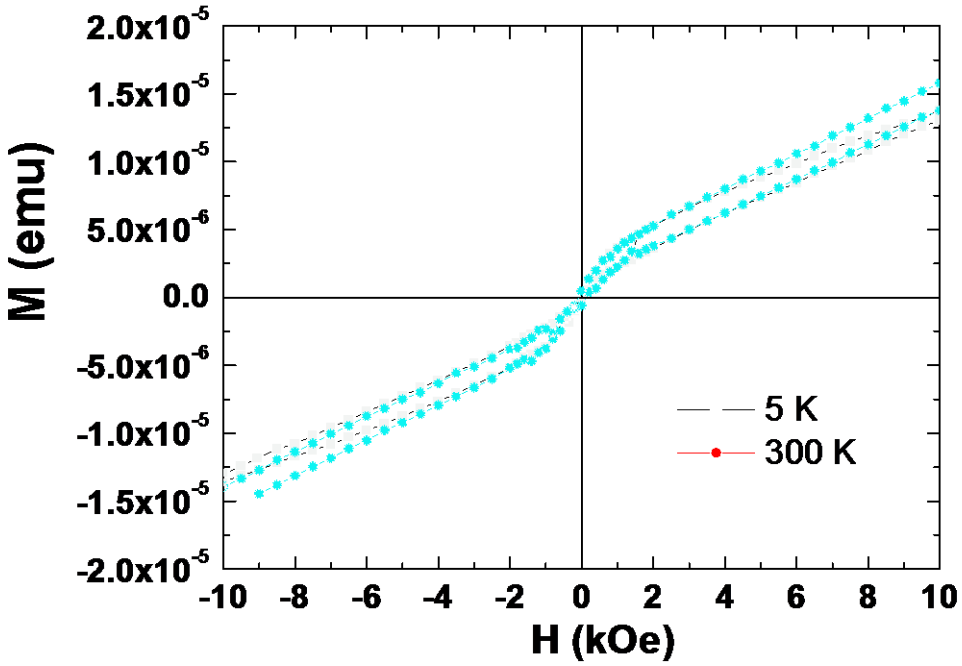

Figure 12 Hysteresis loops for FeAs single crystal taken at 5 and 300K. (Show only for 5K).

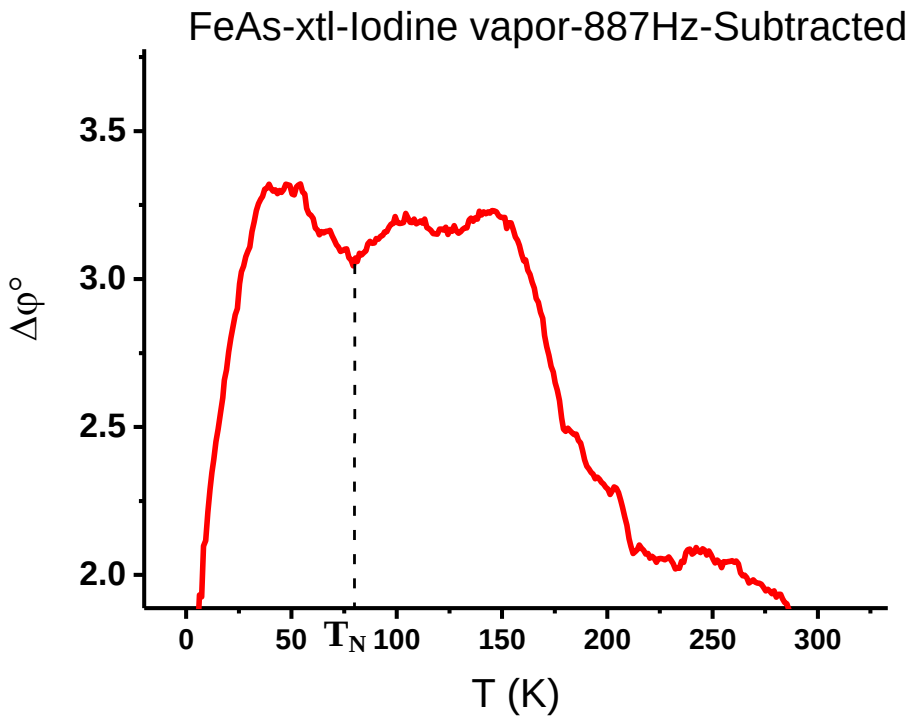

Figure 13 The dependences of the phase shift on temperature shows T_N

3.2 $Fe_{1-x}Co_xAs$ polycrystalline

The dependence of the total susceptibility on the temperature of polycrystalline FeAs shows high signal, more than 10-times the background signal. Therefore; the background signal was ignored (Figure 14).

The measurements of the total susceptibility are shown in figures 15,16,17. We found that the FWHM increase as the frequency increase with increasing Co-concentration. The peak position shifts to a higher temperatures with cobalt concentrations. The comparison between the samples is shown in figure 18. The increase in the transition with (FWHM) indicates increase in the disorder in the spin orientation, eventually leading to a destruction of the helical spin configuration in the parent (FeAs) compound.

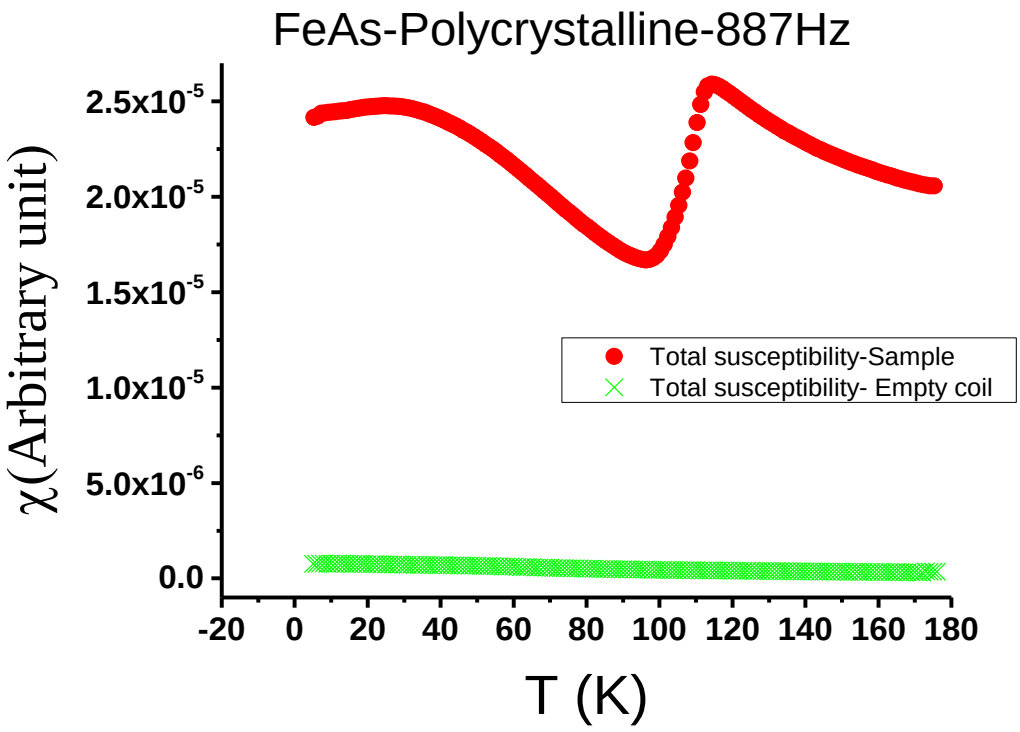

Figure 14 Comparison between Sample and empty coil

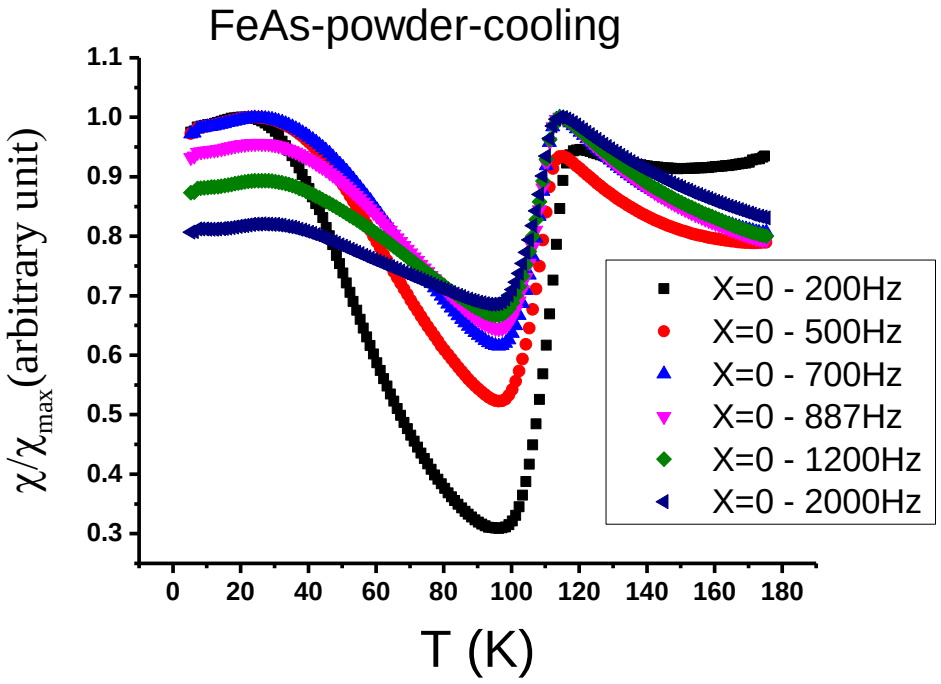

Figure 15 The Normalization of the dependences of the Total Susceptibility on temperature, x=0

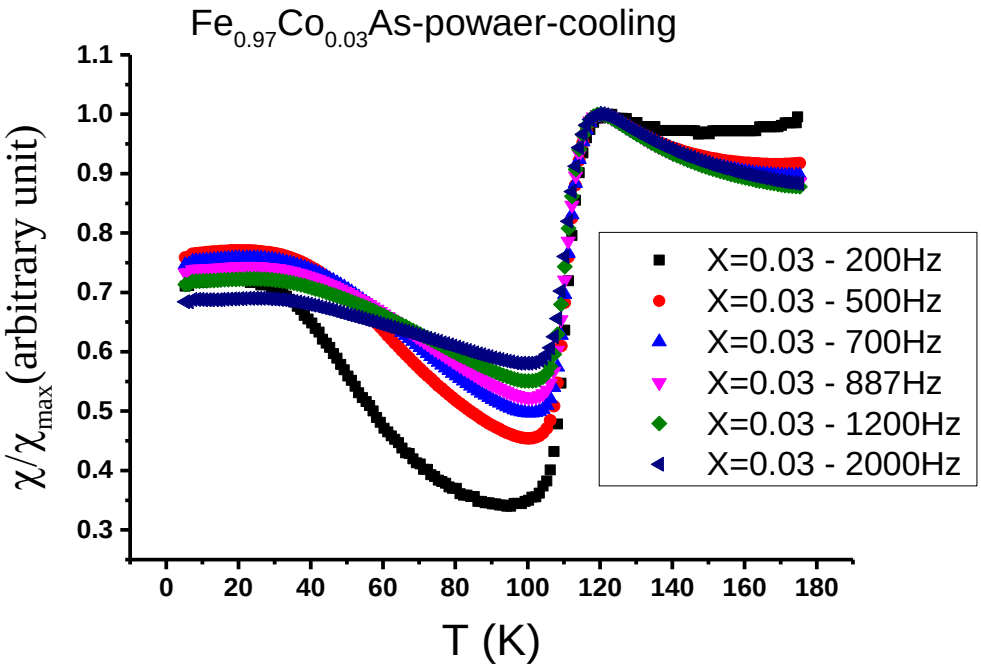

Figure 16 The Normalization of the dependences of the Total Susceptibility on temperature, x=0.03

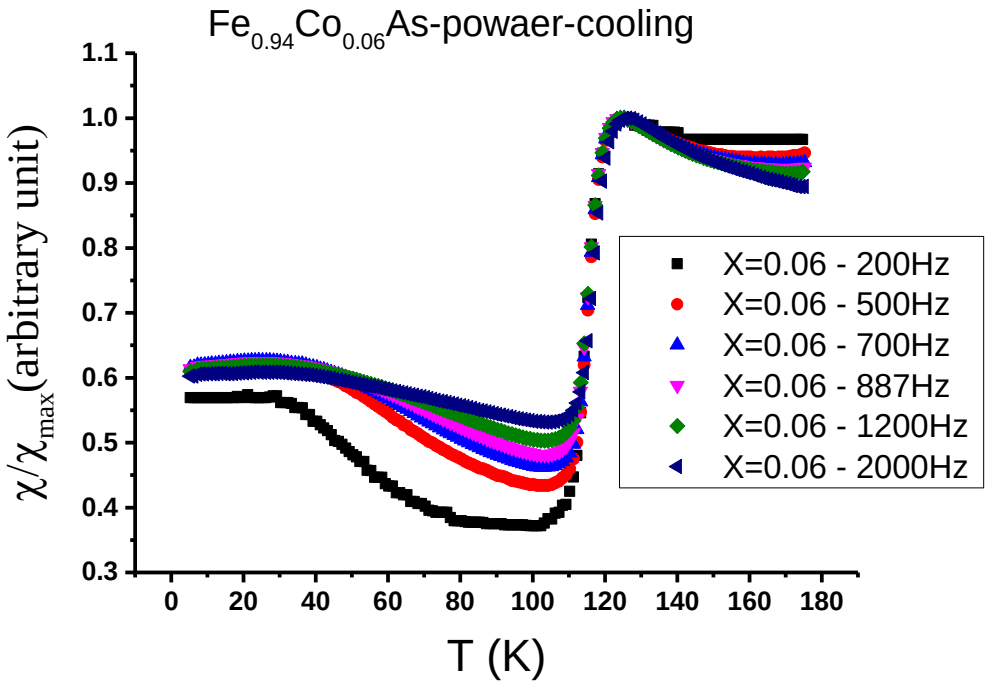

Figure 17 The Normalization of the dependences of the Total Susceptibility on temperature, x=0.06

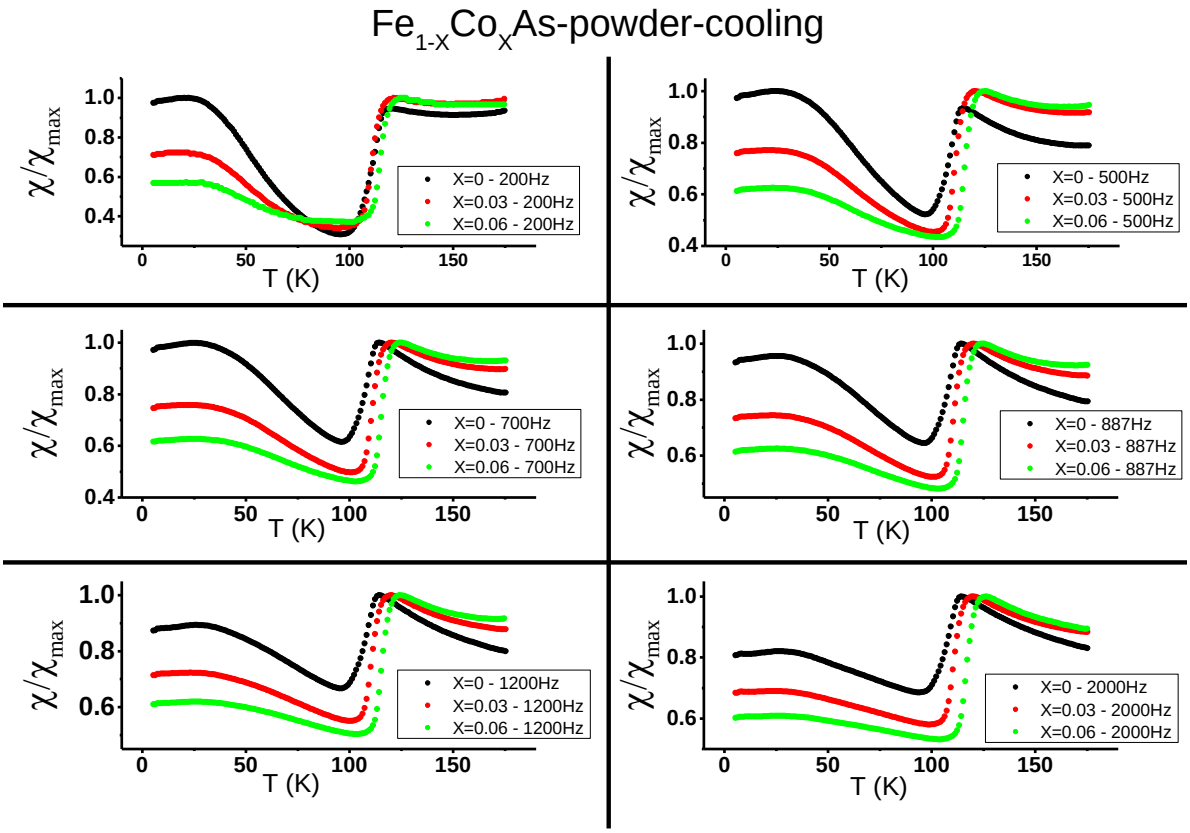

Figure 18 The comparison of the total susceptibility between the samples

CHAPTER 4

The Lag-angle Between the Magnetization and the ac-Field

Ac susceptibility measurements require the application of ac-magnetic field in a primary coil and measures the induced voltage in a set of a secondary pick coils. However, the measured voltage will always lag behind the applied voltage. Since the applied voltage generates ac-magnetic field, and the measured voltage is proportional to the magnetization of the susceptibility of the sample; there will always be a lag between the applied magnetic field and the magnetization. In this Chapter, we present our measurements of the lag angle and its uses in evaluating the activation energy. The ac-Field is given by:

$$H(t) = H_0 + h\cos(\omega t) \qquad (4.1)$$

where h is the amplitude of the driving field. The phase shift θ may occur in magnetization M(t) in respect of H(t) and given by:

$$M(t) = M_0 + m\cos(\omega t - \theta) \qquad (4.2)$$

where θ is the lag-angle $\Delta\varphi$ between the magnetization and the applied ac-field.

The lag-angle $\Delta\varphi$ between the magnetization and the applied ac-field was investigated at different frequencies. The dependence of Lag angle $\Delta\varphi$ on temperature was depicted in figures 19, 20, 21 for $Fe_{1-x}Co_xAs$, where, x=0, 0.03, 0.06 respectively.

In figure 19, we present the results for the parent FeAs compounded. The figure shows measurements of the lag angle between the magnetization and the applied ac-field in the frequency range 100-2000Hz. At low frequency, the peaks gets sharper and shifts towards lower Tp. This indicates lowering in the FWHM. These variations in the position of the peak with frequency indicates the presence of some sort of activation energy for spins to change orientations during the phase transition. These changes will be used to evaluate the activation energy in chapter 5.

Measurements for $Fe_{1-x}Co_xAs$ are shown in Fig 20 and 21. All figures revealed the presence of a peak with a width given as (FWHM) at a given temperature (T_P). The maximum in the lag angle $\Delta\varphi$, the FWHM and the peak temperature T_P may change (in general) with the applied frequency. The position of the maximum ($\Delta\varphi$) decrease when the frequency increase. To simplify comparison, the lag angle $\Delta\varphi$ was normalized by dividing its values by the maximum lag angle at each frequency. The dependence of the normalization Lag angle $\Delta\varphi$ on temperature are shown in figures 22, 23, 24. They exhibit T_P shift to higher values with increasing frequency. In figure 25, we presented the comparison between the various samples which reveal that as x increases the FWHM increase indicating that the helical structure extends slightly into the normal antiferromagnetic state. This is the same result that was found in the previous chapter. T_P reveals decrease as x increase just at low frequency. We conclude that T_P represents the phase transition from paramagnetic state to antiferromagnetic which is also associated with increasing FWHM signaling the destruction of the double c-axis helimagnetic ordering.

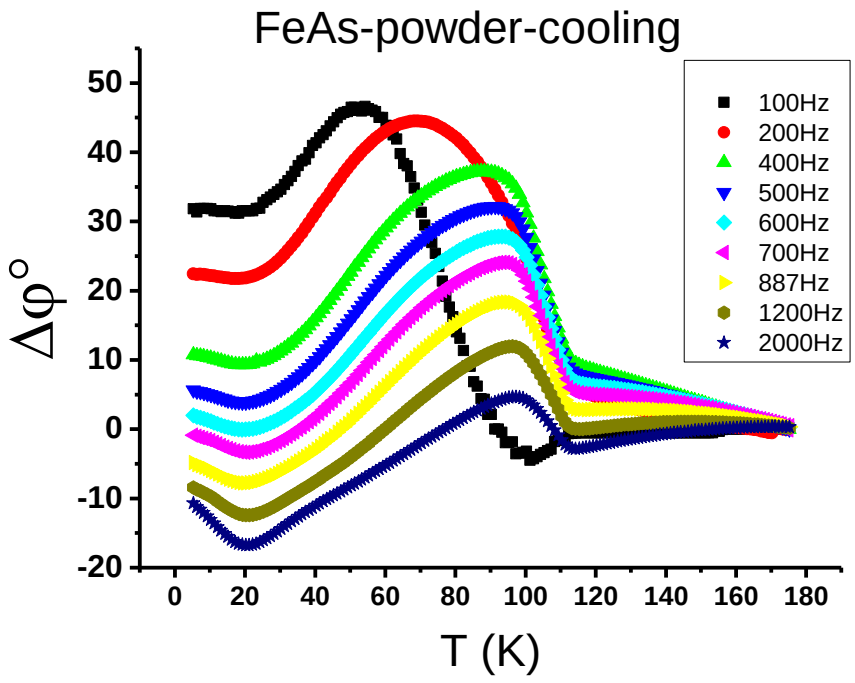

Figure 19 The dependences of the lag-angle Δφ on temperature, x=0

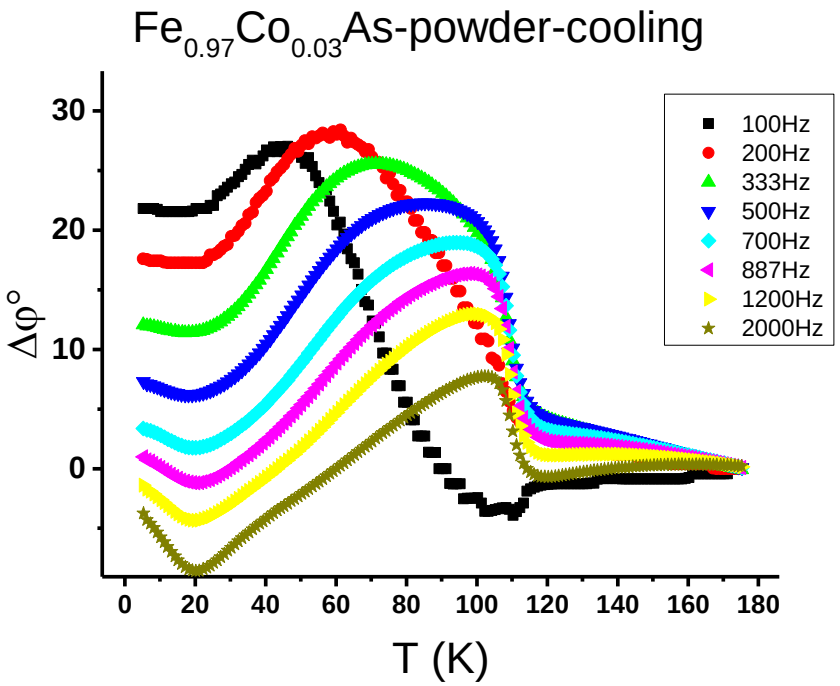

Figure 20 The dependences of the lag-angle Δφ on temperature, x=0.03

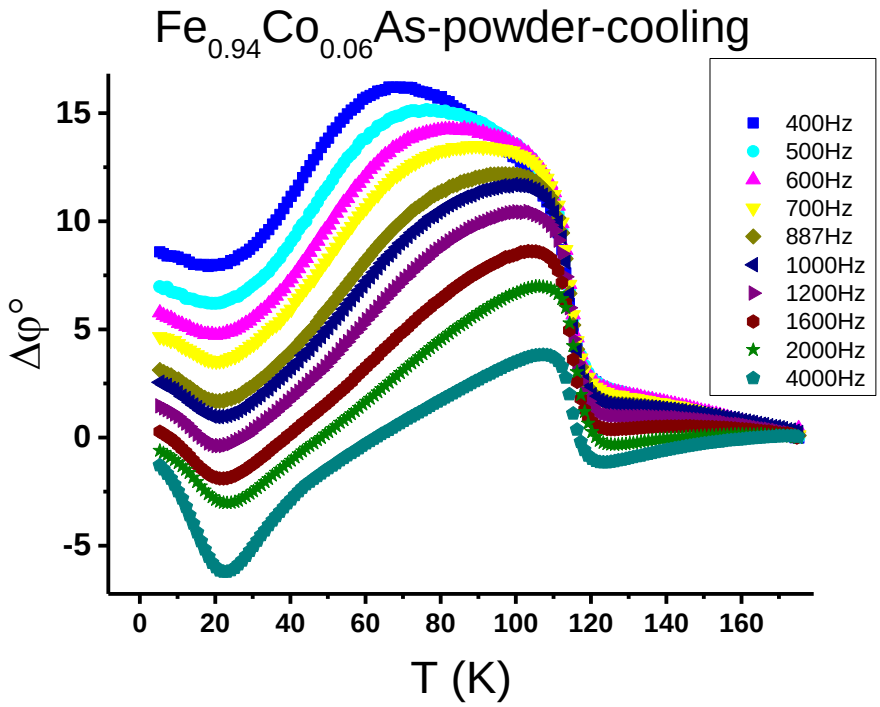

Figure 21 The dependences of lag-angle Δφ shift on temperature, x=0.06

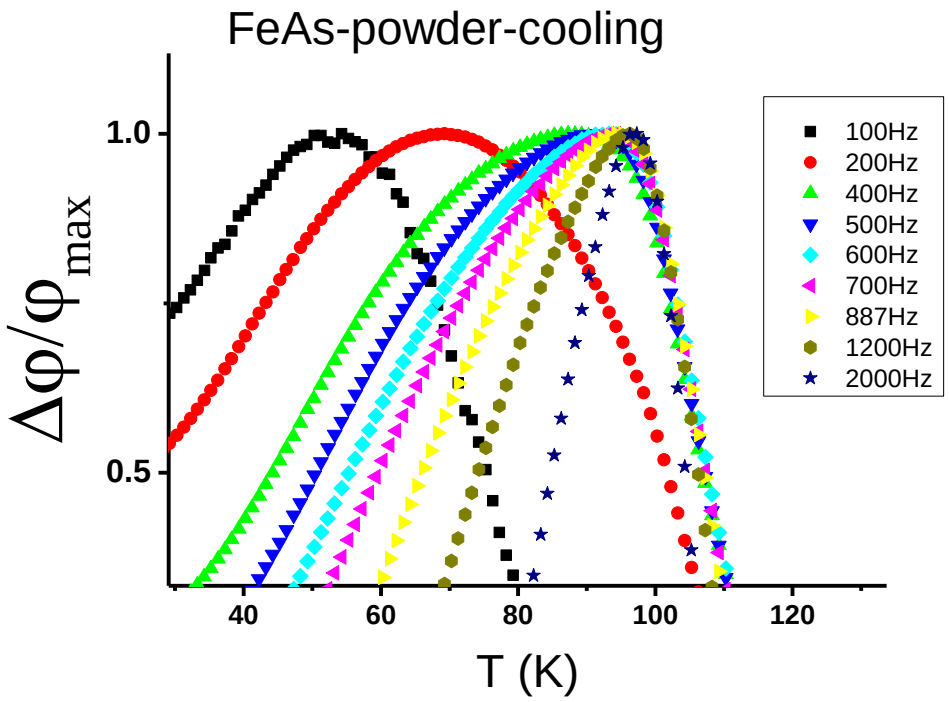

Figure 22 The Normalization of the dependences of the lag-angle Δφ on temperature, x=0

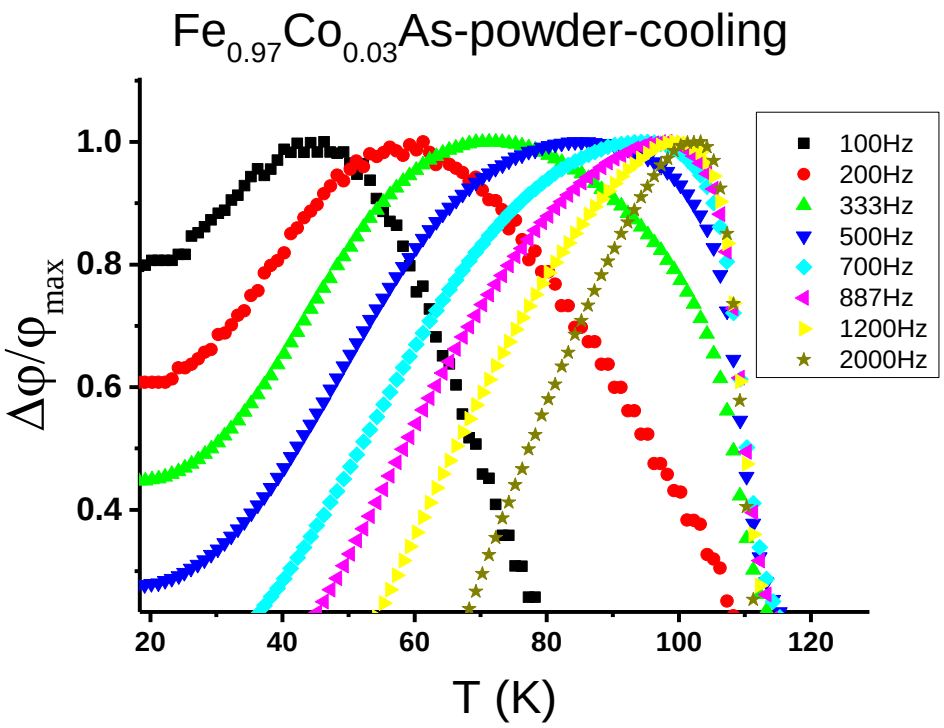

Figure 23 The Normalization of the dependences of the lag-angle Δφ on temperature, x=0.03

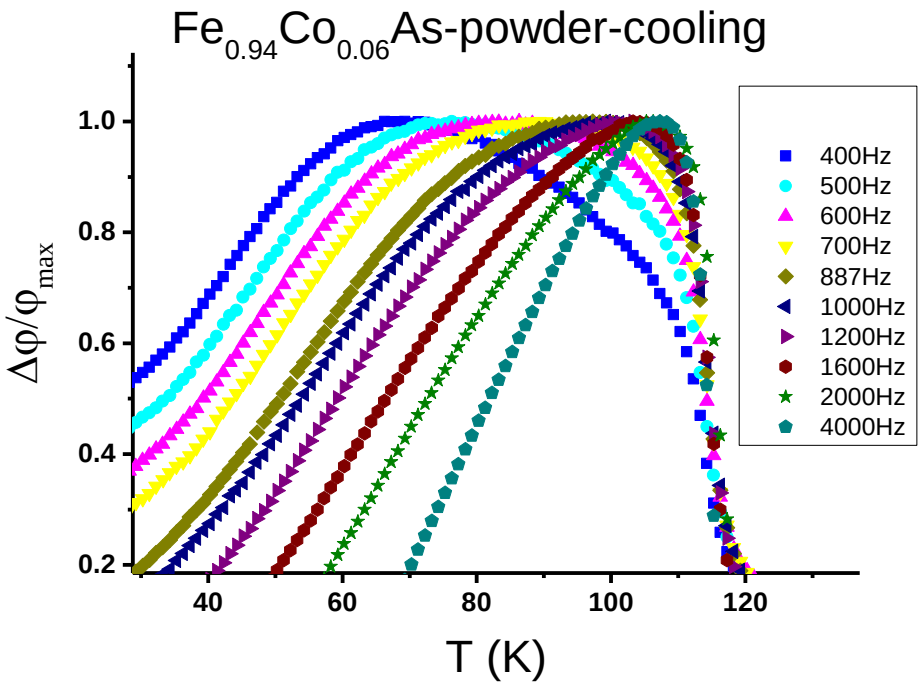

Figure 24 The Normalization of the dependences of the lag-angle Δφ on temperature, x=0.06

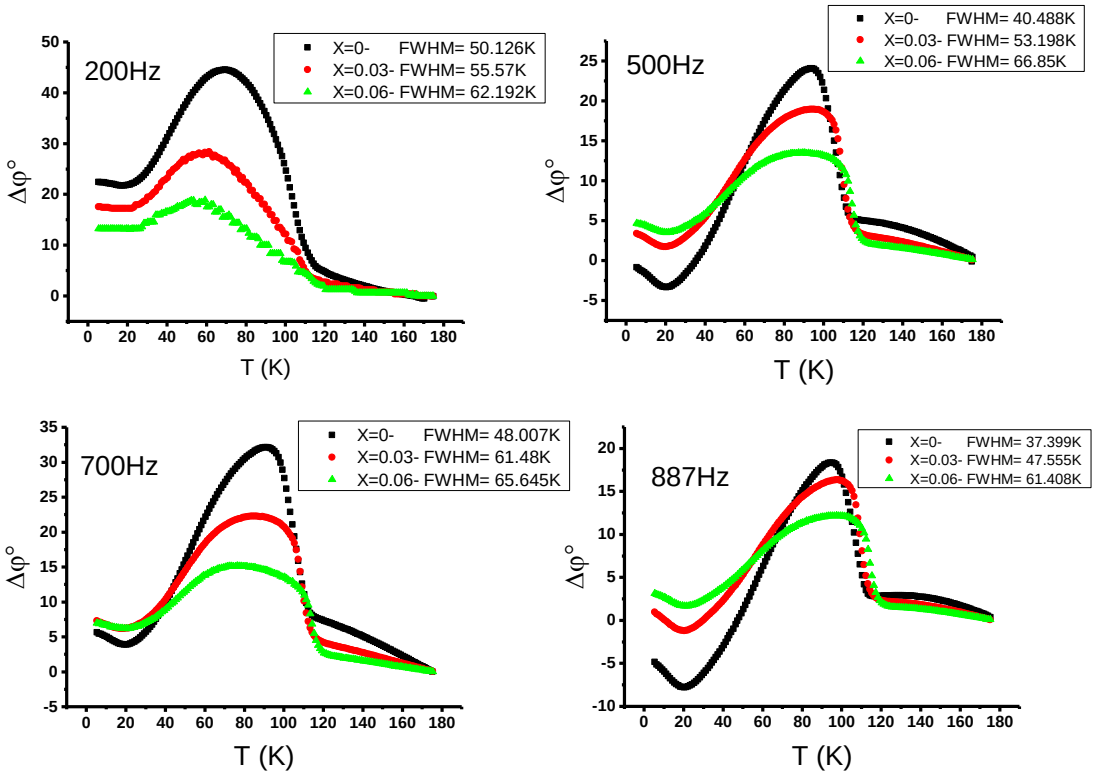

Figure 25 The comparison between the samples

CHAPTER 5

ACTIVATION ENERGY

The activation energy (U_0) is the minimum energy required to reach the transition state. The activation energy can be evaluated using the variation of position of the peak in the ac-susceptibility with frequency using the Arrhenius law (low frequency) [17]. The relaxation time $\tau(T) = 1/f$ is expressed as:

$$\tau(T) = \tau_0 \exp\left(\frac{\Delta E}{k_B T}\right) \qquad (5.1)$$

As the applied magnetic field changes from H to H ± ΔH, magnetization M of a spin system will reach a new equilibrium state after characteristic time τ, called the relaxation time. Relaxation process proceeds through the rotation of magnetic moments, movement of domain walls and other effects. So equation (5.1) convert to:

$$lnf = \frac{-\Delta E}{k_B}\ \frac{1}{\mathrm{T}} + \ln f_0 \qquad (5.2)$$

ΔE is the activation energy. The slope of Arrhenius plot of (lnf vs. $1/T_P$) equal $\frac{-\Delta E}{k_B}$.

The results of the samples are displayed in figures 26 and 27 depend on chapter 4 where discussed the lag angle ($\Delta\varphi$). The comparisons between the samples are shown in figure 26. The plot of lnf vs. $1/T_P$ reveal the linear part at low frequency. Therefore, we consider the Arrhenius plot of (lnf vs. $1/T_P$) just at low frequency to find the activation

energy which is shown in figure 27. The values of activation energy are: $\frac{\Delta E}{k_B}$ = 199.45K=0.017ev, $\frac{\Delta E}{k_B}$ = 150.80K=0.013ev, $\frac{\Delta E}{k_B}$ = 115.84K=0.009ev, for x= 0, 0.03, 0.06, respectively. We found that the activation energy decrease as x increase indicating that helical magnetic structure is becoming easier to destroy. The activation energy data are presented in Table 3.

At higher temperatures, there are deviations from an Arrhenius law. In this range, a Vogel–Fulcher behavior, may describe the data [37-39].

$$\tau(T) = \tau_0 \exp\left(\frac{\Delta E}{k_B(T-T_0)}\right) \qquad (5.3)$$

Where T_0 is the frequency independent "ideal magnetic transition temperature". We found that the peak temperature of the lag angle reach to the saturation state where the saturation value equal T_0 see (Figure 28). Also, we found out that T_0 increase as x increase. The deviation of the activation energy was shown in figures 29 and 30. The values of activation energy are: $\frac{\Delta E}{k_B}$ = 2.1K, $\frac{\Delta E}{k_B}$ = 5.1K, $\frac{\Delta E}{k_B}$ = 7.2K=, for x= 0, 0.03, 0.06 respectively. We noticed that the activation energy increase as x increase as result of increasing T_0 where T_0 related to the strength of the magnetic interaction. These data are presented in Tables 3 and 4 along with other parameters that we evaluate earlier.

Table 3 Some values of the parameters at 500Hz

X	T_P	$\Delta\varphi_{max}$	FWHM	T_K	ΔE
0	90.75K	24.02°	40.49K	115.48K	0.017ev
0.03	84.99K	19.01°	53.19K	119.98K	0.013ev
0.06	76.81K	13.64°	66.85K	123.54K	0.009ev

Table 4 Some values of the parameters at 2000Hz

X	T_P	$\Delta\varphi_{max}$	FWHM	T_K	$\Delta E/K_B$	T_o
0	97.1K	4.5°	28.7K	114.8K	2.1K	97.7K
0.03	101.7K	7.6°	34.1K	119.4K	5.1K	104.5K
0.06	105.2K	7.1°	45.8K	125.3K	7.2K	110.5K

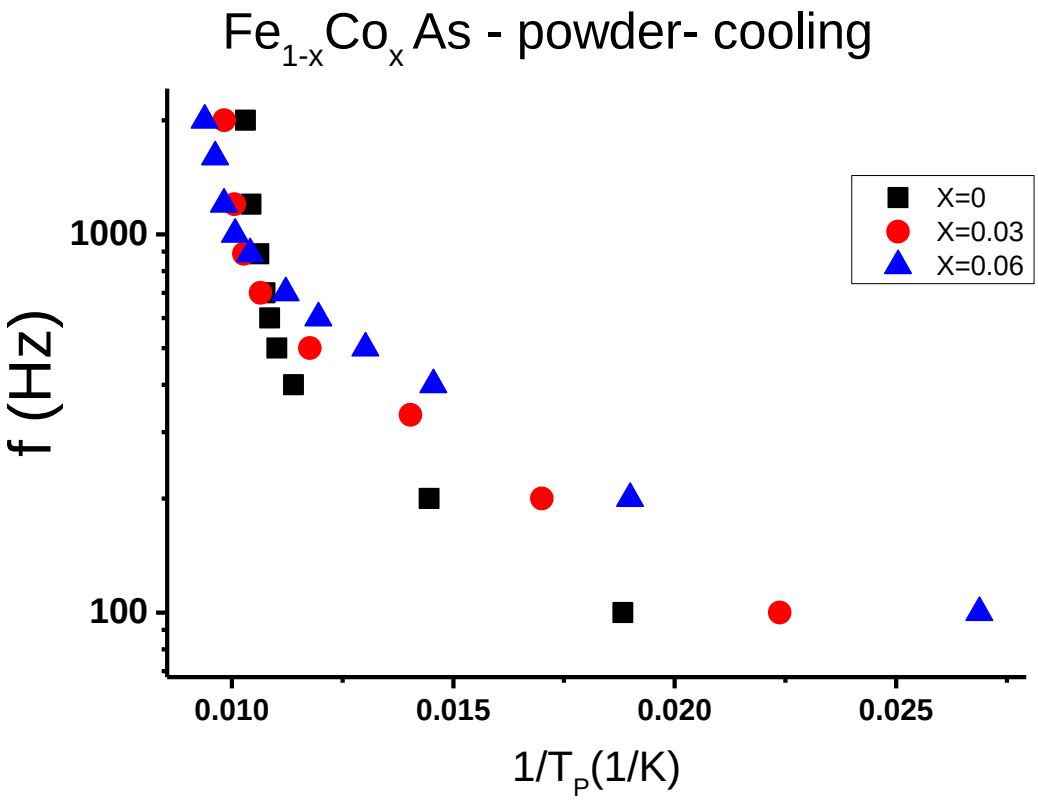

Figure 26 Plot lnf vs. 1/ T_P, x=0, 0.03, 0.06

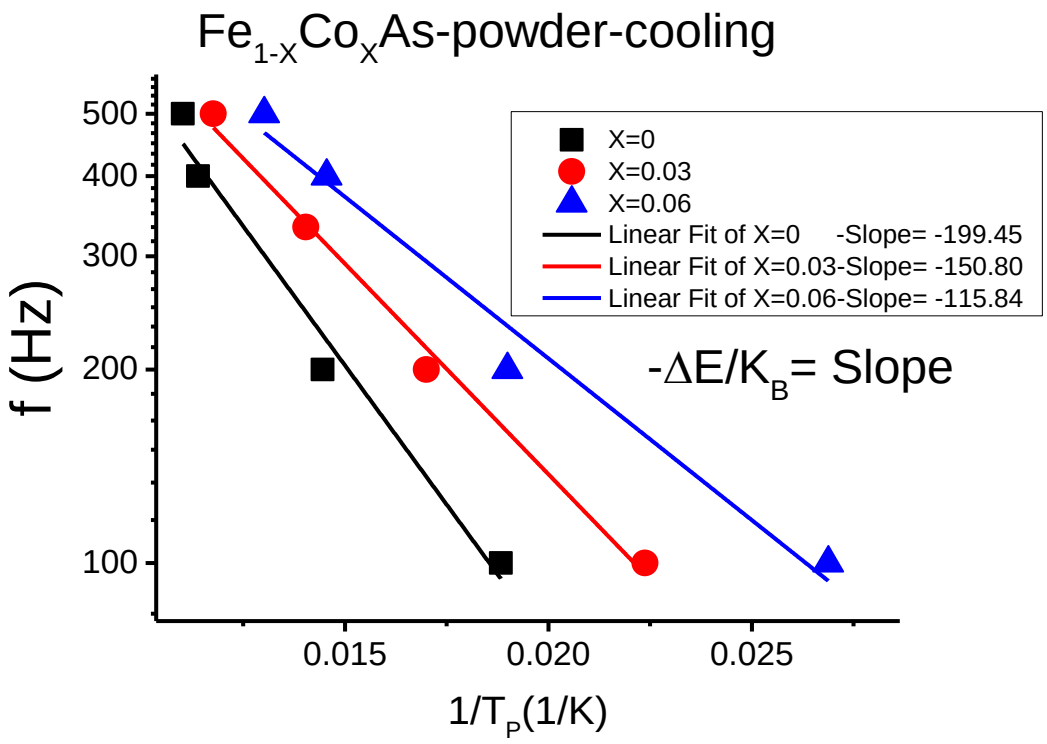

Figure 27 Plot lnf vs. 1/ T_P, x=0, 0.03, 0.06, at Low Frequency

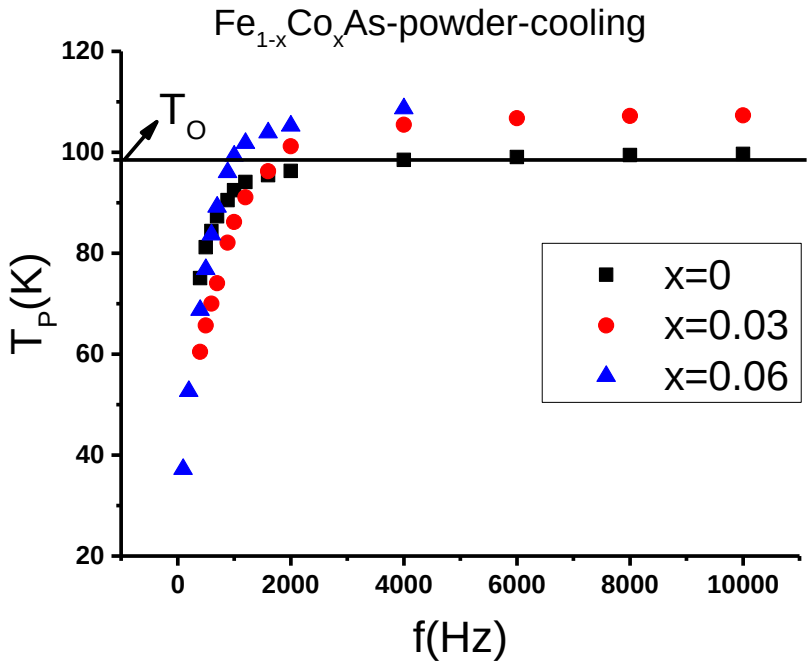

Figure 28 The dependence of T_P on frequency

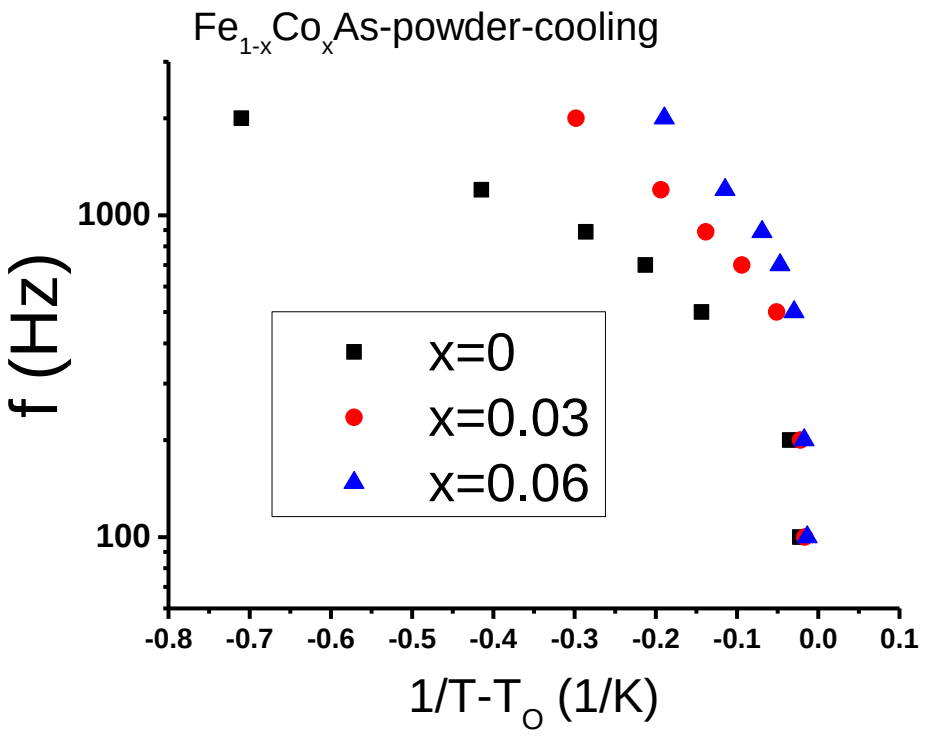

Figure 29 The deviation of the activation energy at high frequency

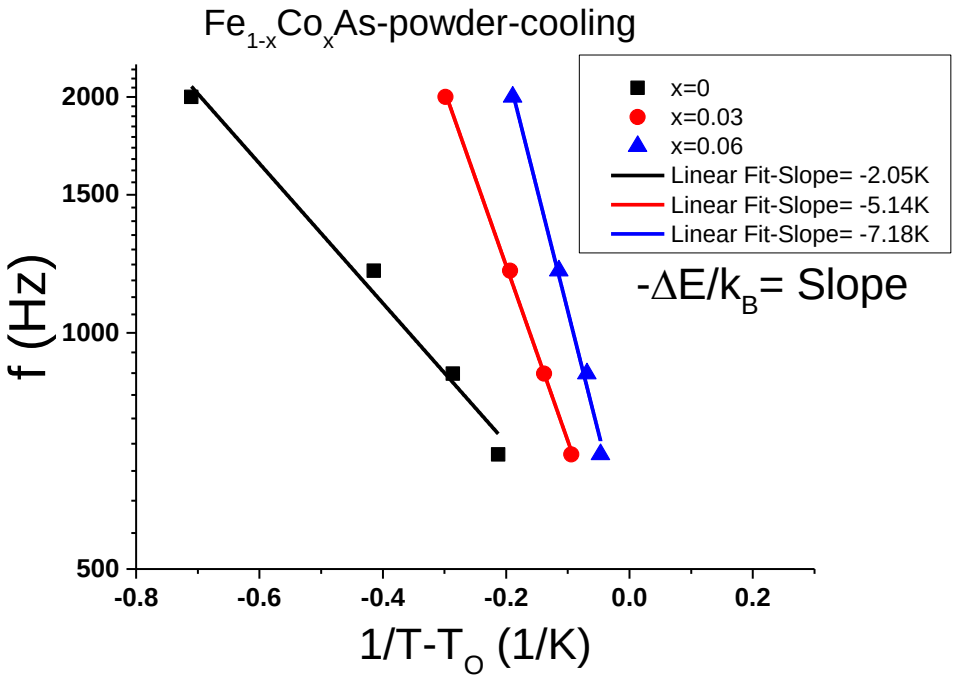

Figure 30 Plot lnf vs. 1/(T_P -T_O), x=0, 0.03, 0.06, at high Frequency

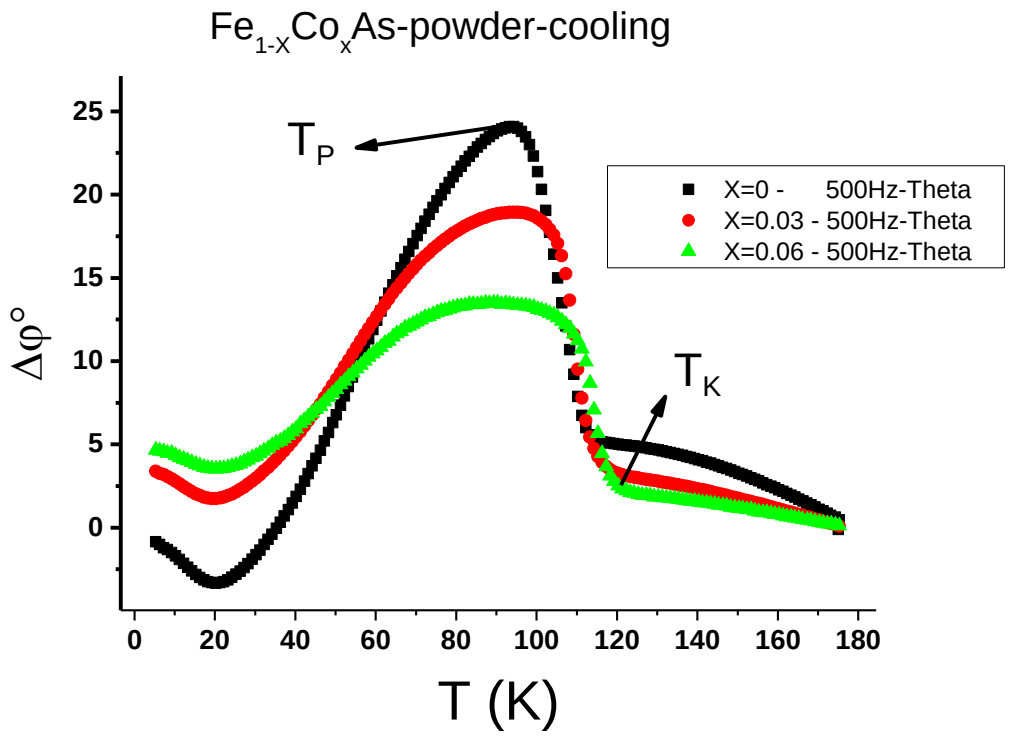

Figure 31 Shows some parameters at 500Hz

CHAPTER 6

CONCLUSION

In this thesis, we investigate the magnetic properties of $Fe_{1-x}Co_xAs$. We found out Cobalt substation in (FeAs) destroys the helical structure of antiferromagnetic and changes the state to the normal antiferromagnetic behaviour.

The measurements of the total susceptibility show that the FWHM increase as the frequency increase in all samples with varying Co concentration. The lag-angle $\Delta\varphi$ between the magnetization and the applied ac-field was investigated at different frequencies. The dependence of Lag angle $\Delta\varphi$ on temperature and frequency, revealed that the FWHM and $\Delta\varphi$ peak temperature T_P increase as the frequency increase, but position of the maximum ($\Delta\varphi$) decrease. Both measurements of the total susceptibility and the lag-angle $\Delta\varphi$ display that the FWHM increase as x increase, indicating that the helical structure extend slightly into normal antiferromagnetic state.

The Arrhenius plot of (lnf vs. $1/T_P$) reveal the linear part at low frequency which used to find the activation energy. The activation energy $\frac{\Delta E}{k_B}$ = 199.45K=0.017ev, $\frac{\Delta E}{k_B}$ = 150.80K=0.013ev, $\frac{\Delta E}{k_B}$ = 115.84K=0.009ev, for x= 0, 0.03, 0.06, respectively. The deviation of the activation energy at high frequency to the Vogel–Fulcher law was explained. The values of activation energy are: $\frac{\Delta E}{k_B}$ = 2.1K, $\frac{\Delta E}{k_B}$ = 5.1K, $\frac{\Delta E}{k_B}$ = 7.2K=, for

x= 0, 0.03, 0.06 respectively. The activation energy increase at high frequency as result of increasing the strength of the coupling interaction in the materials.

References

[1] J.M.D.Coey, “Magnetism and Magnetic Materials,” *Cambridge Univ. Press*, 2009.

[2] C.-G. Stefanita, *Magnetism: Basics and Applications*. 2012.

[3] Y. Kamihara, T. Watanabe, M. Hirano, and H. Hosono, “Iron-Based Layered Superconductor La [O 1 - x F x] FeAs (x) 0 . 05 - 0 . 12) with T c) 26 K,” pp. 3296–3297, 2008.

[4] M. G. K. E. Fylking, Ark. Kemi, “No Title,” vol. No 48, no. B11, 1935.

[5] A. K. Selte, A. Kjekshus, “Magnetic Structure and Properties of FeAs,” *Acta Chem. Scand*, no. A 26, 1972.

[6] K. S. and A. Kjekshus, “The Crystal Structure of FeAs.” pp. 2047–2054, 1969.

[7] M. Morifuji and K. Motizuki, “Theoretical study of double helical magnetic ordering of FeAs,” *J. Magn. Magn. Mater.*, vol. 90–91, pp. 740–742, 1990.

[8] Kouji Segawa and Yoichi Ando, “Magnetic and Transport Properties of FeAs Single Crystals FeAs FeAs,” *J. Phys. Soc. Japan*, vol. 78, no. 10, pp. 10–12, 2009.

[9] T. Frawley, R. Schoonmaker, S. H. Lee, C. Du, P. Steadman, J. Strempfer, K. A, S. J. Clark, T. Lancaster, and P. D. Hatton, “Elucidation of the helical spin structure of FeAs,” pp. 1–10.

[10] E. E. Rodriguez, C. Stock, K. L. Krycka, C. F. Majkrzak, P. Zajdel, K. Kirshenbaum, N. P. Butch, S. R. Saha, J. Paglione, and M. A. Green, “Noncollinear spin-density-wave antiferromagnetism in FeAs,” vol. 134438, pp. 1–6, 2011.

[11] D. Gonzalez-alvarez, “FeAs : Heat capacity , enthalpy increments , other thermodynamic properties from 5 to 1350 K , and magnetic transition a,” pp. 363–373, 1989.

[12] A. F. A. K. Selte, A. Kjekshus, S. Aaby, “Magnetic Structures and Properties of Cr1-tCotAs and Fe1-tCotAs.” pp. 810–816, 1975.

[13] B. D. Cullity and C. D. Graham, *Introduction to Magnetic Materials*, Second. Canada: Wiley, 2009.

[14] D. J. Griffiths, *Introduction to Electrodynamics*, Thired edi. United States of America: Printed-Hall, 1999.

[15] S. CHIKAZUMI, *Physics of Ferromagnetism*, SECOND. New York: OXFORD, 1997.

[16] M. Ba[a]anda, “AC Susceptibility Studies of Phase Transitions and Magnetic Relaxation : Conventional , Molecular and Low-Dimensional Magnets,” vol. 124, no. 6, pp. 964–976, 2013.

[17] D. R. Lide, “Magnetic susceptibility of the elements and inorganic compounds,” *CRC Handb. Chem. Phys. 86*, pp. 130–135, 2000.

[18] D. Martien, “Introduction to AC Susceptibility.”

[19] M. Nikolo, “A guide to alternating current susceptibility measurements and alternating current susceptometer design.” American Journal of Physics, pp. 57–65, 1994.

[20] and J. P. J. R. Jeries, N. P. Butch, H. Cynn, S. R. Saha, K. Kirshenbaum, S. T. Weir, Y. K. Vohra, “No Title,” vol. arXiv:1012, no. .1391v1, 2010.

[21] A. Błachowski, K. Ruebenbauer, J. Ż, and Z. Bukowski, “Magnetic anisotropy and lattice dynamics in FeAs studied by Mössbauer spectroscopy,” pp. 1–21, 2013.
[22] R. J. M. and a. 1. G. S. Nandi, M. G. Kim, a. Kreyssig, R. M. Fernandes, D. K. Pratt, a. Thaler, N. Ni, S. L. Budko, P. C. Canfield, J. Schmalian, “No Title,” *Phys. Rev. Lett.*, vol. 104, pp. 1–4, 2010.
[23] M. Ba[a]anda, “AC Susceptibility Studies of Phase Transition and Magnetic Relaxation,” vol. 124, pp. 964–976, 2013.
[24] H. Salamati and P. Kameli, “AC susceptibility of YBa2Cu3O7- δ superconducting thin film in a perpendicular field,” vol. 0, pp. 1–15.
[25] B. Sr, O. Cacu, and M. I. Youssif, “Effects of Flux Creep in Bulk and Single Crystals of,” no. 25, pp. 171–179, 2002.
[26] M. Nikolo, X. Shi, E. S. Choi, J. Jiang, J. D. Weiss, and E. E. Hellstrom, “Frequency Dependent Flux Dynamics and Activation Energies in Pnictide Bulk (Ba0.56K0.44)Fe2As2 Superconductor,” *Phys. Procedia*, vol. 67, pp. 939–944, 2015.
[27] M. Ba, K. Falk, K. Griesar, Z. Tomkowicz, and W. Haase, “Characterization of magnetic ordering in porphyrin-based molecular magnets [Mn (R) TPP][TCNE] (R " OC H , F , CN),” vol. 205, pp. 14–26, 1999.
[28] W. Haase, “Single-chain magnet features in 1D [MnR4TPP] [TCNE] compounds,” no. July, 2011.
[29] P. D. Allen and T. G. S. Pierre, “Low-frequency low- ¢ eld magnetic susceptibility of ferritin and hemosiderin,” vol. 1500, pp. 186–196, 2000.
[30] “Disordered magnetism and spin glasses,” vol. 158, pp. 606–610, 1996.
[31] D. V Szabo, “Effect of dipolar and exchange interactions on magnetic blocking of maghemite nanoparticles,” vol. 323, pp. 1998–2004, 2011.
[32] K. A. Z. A. F. Salem, “Magnetic Properties of FeAs Single Crystal,” pp. 1185–1188, 2013.
[33] C. W. Looney and E. Kline, “Resistivity and Susceptibility Measurements in a Helium-Gas System,” pp. 0–65, 2014.
[34] S. Yonezawa, T. Higuchi, Y. Sugimoto, C. Sow, and Y. Maeno, “Compact AC Susceptometer for Fast Sample Characterization down to 0.1 K,” vol. 1, no. August, pp. 1–6, 2015.
[35] L. Cevey, “Miniature AC susceptometer,” pp. 1–3, 2009.
[36] Selte, K. A. R. I., and A. R. N. E. Kjekshus. "Structural and magnetic properties of CoAs." Acta. Chem. Scand. (1971).
19229–19240, 2014.
[37] M. Sattig, S. Reutter, F. Fujara, and M. Werner, “NMR studies on the temperature-dependent dynamics of confined water,” *Phys. Chem. Chem. Phys.*, vol. 16, pp. 19229–19240, 2014.
[38] T. Hao, “Unveiling the relationships among the viscosity equations of glass liquids and colloidal suspensions for obtaining universal equations with the generic free volume concept,” *Phys. Chem. Chem. Phys.*, vol. 17, pp. 21885–21893, 2015.
[39] P. Review, T. Guwahati, and S. State, “Magnetic compensation , field-dependent magnetization reversal , and complex magnetic ordering in Co 2 TiO 4,” no. December 2015, 2016.

Vitae

Name	Fares Subait Hadi Obad
Nationality	Yemen
Date of Birth	3/20/1985
Email	faresobad@gmail.com
Address	HADRAMOUT - YEM

Academic Background : -

BSc. In Physics – Umm Al-Qura University with first honor 2009

- KFUPM- Physics Department 2017

- Seminar & Workshops :

1- Measurement Of Potassium (k-40) In Soil Using Gamma Ray Spectroscopy Jan , 2016

2- Measurement Of ac -Susceptibility In MgB2-CuF2 Superconductor Feb , 2016

3- Elemental Analysis of Coffee Sample Using Laser Induced Breakdown Mar , 2016

4- Quantum Tunneling at Room Temperature Using Tunnel Diode Dec , 2016

5- Design and usage of the susceptometer for AC Susceptibility 2016-2017